UNIVERSIDADE DE LISBOA

FACULDADE DE CIÊNCIAS

DEPARTAMENTO DE BIOLOGIA VEGETAL

Exploring the role of metabolism in the differentiation and maturation of human pluripotent stem cell derived cardiomyocytes

Mestrado em Biologia Molecular e Genética

Patricia Rodrigues Duarte

Dissertação orientada por:

Orientador externo: Doutora Margarida Serra, Instituto de Biologia Experimental e Tecnológica (IBET) e Instituto de Tecnologia Química e Biológica António Xavier, Universidade Nova de Lisboa (ITQB-NOVA), Oeiras

Orientador interno: Prof. Doutora Anabela Silva, Departamento de Biologia Vegetal da Faculdade de Ciências da Universidade de Lisboa (FCUL), Lisboa

2016

Acknowledgments

I would like to acknowledge all the people directly or indirectly involved in this thesis.

To Dr. Paula Alves, for giving me the opportunity to do my master thesis at Animal Cell Technology Unit at ITQB/IBET and for the good working conditions offered.

To Dr. Margarida Serra, for the opportunity to partake in this project. For her guidance, encouragement and support.

To Prof. Dr. Anabela Silva for accepting to be my internal advisor and for being available to help during my master thesis work.

To Cláudia and Alex, for teaching me most of what I learnt throughout this year, for the scientific discussions. For the great team spirit, encouragement, advice and for being good friends throughout this year.

To all the ACTU colleagues, for the good working environment, friendship and help during this year.

Aos meus pais, pelo apoio constante e por me terem proporcionado todas as condições para que fosse possível alcançar mais uma etapa.

Preface

The current master thesis was performed at the Animal Cell Technology Unit (ACTU), IBET / ITQB-NOVA, within the scope of the projects CARDIOSTEM (MITP-TB/ECE/0013/2013) and CardioRegen (HMSP-ICT/0039/2013) funded by Fundação para a Ciência e Tecnologia (FCT) and iNOVA4Health (UID/Multi/04462/2013) a program supported by FCT/Ministério da Educação e Ciência.

Part of the work of this thesis has been included in two articles (one submitted and another in final preparations) and presented as oral and poster communications at international conferences.

Submitted Article:

Cláudia Correia, Alexey Koshkin, Patrícia Duarte, Dongjian Hu, Ana Teixeira, Ibrahim Domian, Margarida Serra, Paula M. Alves. "Unveiling the impact of metabolic substrate availability on maturation of human induced pluripotent stem cells derived cardiomyocytes: an "-Omics" driven approach" (submitted to Cell Metabolism, September, 2016)

Oral Presentation:

Cláudia Correia, Alexey Koshkin, Patrícia Duarte, Dongjian Hu, Ana Teixeira, Ibrahim Domian, Margarida Serra, Paula M. Alves. Using "-omics" tools to improve differentiation and maturation of cardiomyocytes derived from human pluripotent stem cells. ESGCT - ISSCR Collaborative Congress, October 2016. Florence, Italy.

Poster Presentation:

Cláudia Correia, Alexey Koshkin, Madalena Carido, Patrícia Duarte, Marcos Sousa, Catarina Brito, Ana Teixeira, Margarida Serra, Paula M Alves. Integrated strategies for the production, maturation and storage of functional cardiomyocytes derived from human pluripotent stem cells, Cell Culture Engineering XV, Engineering Conferences International, May 2016, Palms Spring, LA, USA.

Abstract

The immature phenotype of human pluripotent stem cell derived cardiomyocytes (hPSC-CM) is currently the main drawback limiting the potential of these cells for applications in cell therapy and pre-clinical research. Herein, it was assessed whether alteration of hPSC-CM culture medium composition to mimic *in vivo* substrate availability during cardiac development would induce hPSC-CM maturation *in vitro*.

Initial qualitative proteomic characterization of both stem cell and differentiated cultures revealed that although hPSC-CMs remain highly glycolytic, like their pluripotent counterparts, there is an evident development in oxidative metabolic machinery, together with enrichment in cardiac markers, during differentiation to a cardiac lineage. Parallel labeling experiments and ^{13}C-MFA were used for the estimation of intracellular flux distributions, which coupled with structural analysis allowed to elucidate the impact of distinct carbon sources in the metabolic profile and maturation status of hiPSC-CMs. Culture of hiPSC-CMs in media with distinct carbon sources (glucose, lactate, fatty acids and galactose) proved that hiPSC-CMs exhibit remarkable metabolic plasticity, being able to shift to an oxidative metabolism, in the absence of glucose. From the assorted selection of media tested, cell culture in fatty acid medium supplemented with galactose was the most efficient in improving hiPSC-CMs maturation, as cells display an oxidative metabolism and show an elongated morphology with highly organized sarcomeric structures. Furthermore, galactose improved fatty acid oxidation by increasing oxidative capacity thus preventing lipotoxic effects of fatty acid accumulation. In standard glucose rich medium, hiPSC-CMs maintain a fetal-like metabolic profile and display features that resemble pathogenic hypertrophy.

This thesis reports for the first time not only a metabolic network model of hiPSC-CMs cultured in distinct media, but also important insights on how substrate change modulates metabolic and structural maturation of hiPSC-CMs. As such, this work represents a relevant step forward in time efficient maturation of hiPSC-CMs, facilitating the use of this promising cell type in clinical and pre-clinical applications.

Keywords: Human pluripotent stem cells derived cardiomyocytes (hPSC-CMs); Cardiomyocyte maturation; Fatty Acids; Galactose; Metabolic Flux Analysis

Resumo

Atualmente, e apesar dos grandes avanços na medicina, as doenças cardiovasculares continuam a ser a principal causa de morte a nível mundial. Muitas destas doenças, como por exemplo o enfarte do miocárdio, estão associadas a uma grande perda permanente de cardiomiócitos, uma população celular não proliferativa e terminalmente diferenciada. Assim, dos tratamentos existentes apenas o transplante cardíaco permite compensar tanto a perda celular como restaurar de forma eficiente a função cardíaca. No entanto, a implementação desta intervenção cirúrgica como tratamento convencional é restringida pelo número limitado de órgãos compatíveis doados.

A capacidade de proliferação ilimitada das células estaminais pluripotentes humanas (hPSC do acrónimo inglês *human pluripotent stem cell*), em conjunto com protocolos de diferenciação direcionada eficientes, permitem a produção de vários tipos específicos de células humanas, incluindo cardiomiócitos. Estas células podem ser usadas numa vasta panóplia de aplicações tal como, medicina regenerativa, rastreio de novos medicamentos ou como modelo celular para avaliar o desenvolvimento e progressão de várias doenças. Apesar do progresso alcançado ao longo dos anos no aumento da eficiência dos protocolos de diferenciação, a população final de cardiomiócitos derivados de hPSC (hPSC-CMs) obtida apresenta um fenótipo imaturo quer em termos de estrutura, expressão génica, metabolismo ou electrofisiologia. Por isto, o estado imaturo dos hPSC-CMs é atualmente o principal fator a limitar o potencial destas células em terapia celular e investigação pré-clinica.

Portanto, o objetivo deste estudo centra-se na avaliação do impacto da alteração da composição do meio de cultura dos hPSC-CMs, por forma a mimetizar os substratos disponíveis durante o desenvolvimento *in vivo* do coração humano, na maturação de hPSC-CMs *in vitro*.

Duas linhas de células estaminais, uma de células estaminais embrionárias humanas (hESC) e outra de hPSC induzidas (hiPSC), foram diferenciadas usando um protocolo recentemente implementado para a diferenciação direcionada de cardiomiócitos em mono-camadas bidimensionais. Análise por citometria de fluxo permitiu garantir a eficiência da metodologia aplicada assim como determinar a pureza da população de cardiomiócitos obtida. Adicionalmente, análise qualitativa do proteoma total de ambas as linhas de células estaminais, antes e após diferenciação, revelou um enriquecimento significativo, em funções biológicas relacionadas com a função cardíaca, após 15 dias de diferenciação. Por outro lado, a análise das principais vias metabólicas mostrou um enriquecimento acentuado em vias como

fosforilação oxidativa, ciclo do TCA, glicólise e β-oxidação de ácidos gordos, após 15 dias de diferenciação. A análise destes resultados revela que durante a diferenciação de células estaminais para uma linhagem cardíaca existe um desenvolvimento em termos de maquinaria metabólica oxidativa, apesar de tanto as hPSC como os hPSC-CMs se manterem principalmente glicolíticos. Deste modo procedeu-se com um estudo metabólico detalhado para avaliar a possível existência de uma relação entre a fonte de carbono disponível no meio de cultura e o perfil metabólico das células.

Após 15 dias de diferenciação, hiPSC-CMs foram mantidos durante mais 20 dias em meio de cultura sem glucose mas suplementado quer com: i) ácidos gordos (FAM), ii) galactose e ácidos gordos (GFAM), iii) lactato durante os primeiros 10 dias seguido de uma troca para galactose e ácidos gordos durante o restante tempo em cultura (LACM&GFAM), além da condição controlo em meio rico em glucose (GLCM). Várias técnicas de metabolómica como HPLC e GC-MS, assim como análise estrutural recorrendo a microscopia de imunofluorescência, foram usadas ao longo da cultura, para avaliar o impacto do uso de fontes de carbono distintas no perfil metabólico e estrutural de hiPSC-CMs.

Uma primeira análise dos dados metabólicos confirmou que hiPSC-CMs em GLCM, mantêm um perfil metabólico dependente de glicólise anaeróbica sem qualquer melhoria na capacidade oxidativa ao longo do tempo em cultura. Este resultado foi comprovado pela taxa de produção de lactato elevada, do qual cerca de 90% advém da metabolização de glucose, e pela fração inalterada de incorporação em intermediários do ciclo do TCA. No entanto, na ausência de glucose, hiPSC-CMs demonstraram uma plasticidade metabólica notável ao consumirem as fontes de carbono distintas suplementadas no meio. Por outro lado, nestes meios sem glucose não se verifica a dependência de glicólise anaeróbica, visto que em nenhuma destas condições houve produção de lactato. Estes resultados sugerem que quando o principal substrato disponível no meio de cultura é glucose, o consumo preferencial deste substrato restringe os hiPSC-CMs a um metabolismo glicolítico. Portanto, o desenvolvimento em termos de maquinaria metabólica durante a diferenciação de hiPSC-CMs, verificado através da análise do proteoma total, poderá refletir uma adaptação inerente dos hiPSC-CMs para o consumo de diversas fontes de carbono e transição para um metabolismo oxidativo.

Para uma caracterização mais detalhada das alterações metabólicas em hiPSC-CMs, as taxas de consumo e produção de metabolitos assim como os dados de incorporação de isótopos ^{13}C foram integrados num modelo da rede metabólica celular, através de ^{13}C-MFA não estacionário. Esta técnica baseia-se no recurso a simulação computacional para estimar um conjunto de fluxos metabólicos intracelulares que minimizem a variância da soma dos

quadrados dos resíduos entre os valores previstos pelo modelo e os medidos experimentalmente. Os modelos metabólicos obtidos ao final do tempo de cultura confirmam os resultados preliminares, de que: i) em GLCM, os hiPSC-CMs permanecem principalmente glicolíticos, no qual a maior parte do piruvato citosólico é desviado para a produção de lactato; ii) nas restantes condições se verifica a transição para um metabolismo oxidativo, com um aumento significativo na contribuição do ciclo de TCA e da β-oxidação de ácidos gordos. Todavia, em FAM, a maior parte dos ácidos gordos que entram na célula são desviados para acumulação nas reservas internas (gotículas lipídicas). Um resultado confirmado com recurso a um *kit* comercial para a quantificação destas reservas, o que justifica a baixa viabilidade observada nas células cultivadas neste meio dado o efeito tóxico da acumulação excessiva de lípidos.

Da seleção de diferentes meios testados, a cultura em meio suplementado com galactose e ácidos gordos (GFAM) provou ser a mais eficiente a promover a maturação de hiPSC-CMs *in vitro*. Aqui, os hiPSC-CMs além de serem caracterizados por um perfil metabólico principalmente oxidativo apresentam também uma morfologia alongada e estruturas sarcoméricas com um elevado nível de organização. Todos estes fatores referidos são característicos de cardiomiócitos humanos adultos. Adicionalmente, a presença de galactose melhorou a oxidação de ácidos gordos ao aumentar a capacidade oxidativa total, prevenindo desta forma os efeitos tóxicos da acumulação de lípidos. Pelo contrário, os hiPSC-CMs mantidos na condição controlo, ou seja em meio rico em glucose (GLCM), apresentam um metabolismo glicolítico, tal como cardiomiócitos fetais, além de que possuem uma morfologia arredondada, área celular maior e sarcómeros desorganizados, estando todas estas características associadas a hipertrofia patológica. Estes resultados evidenciam a importância do papel regulatório do metabolismo numa variedade ampla de funções celulares.

Neste estudo é reportado pela primeira vez um modelo da rede metabólica de hiPSC-CMs cultivados com distintas fontes de carbono, obtido através de ^{13}C-MFA não estacionário, assim como, é explorado o nível ao qual esta mudança na disponibilidade de substratos regula a maturação metabólica e estrutural dos hiPSC-CMs. O protocolo de maturação estabelecido neste estudo apresenta vantagens técnicas e económicas em relação às abordagens existentes, dada a sua simplicidade (uma simples mudança de meio de cultura) e facilidade de aplicação (não requer equipamento específico ou adição de fatores/químicos caros). De notar que, 10 dias de cultura em GFAM foi suficiente para promover um nível de maturação metabólica e estrutural dos hiPSC-CMs comparável ao que tem sido reportado na literatura em culturas de longo prazo.

No cômputo geral, a metodologia aqui desenvolvida constitui um avanço relevante no desenvolvimento de estratégias eficientes de maturação de hiPSC-CMs, facilitando a transferência de hiPSC-CMs para aplicações em terapia celular, testes de toxicidade, descoberta de novos medicamentos e modelos celulares de doenças cardíacas.

Palavras-chave: cardiomiócitos derivados de células estaminais pluripotentes humanas (hPSC-CMs); maturação de cardiomiócitos; ácidos gordos; galactose; análise de fluxo metabólico.

Index

List of Figures

List of Tables

Abbreviation list

3-HaCoA	3-hydroxyacyl CoA
3-KaCoA	3-ketoacyl CoA
3PG	3-Phosphoglyceric acid
AcCoA	Acetyl-CoA
ADP	Adenosine diphosphate
AKG	Alpha-ketoglutarate
ALA	Alanine
ARG	Arginine
ASP	Aspartate
ATP	Adenosine triphosphate
BSA	Bovine serum albumin
CIT	Citrate
CMs	Cardiomyocytes
CO2	Carbon dioxide
cTnI	Cardiac muscle troponin I
cTnT	Cardiac muscle troponin T
CYS	Cysteine
DHAP	Dihydroxyacetone phosphate
E4P	Erythrose 4-phosphate
EDTA	Ethylenediaminetetraacetic acid
eGFP	Enhanced green fluorescent protein
EMU	Elementary metabolic unit
END-2	Visceral endoderm-like cell line
F6P	Fructose-6-phosphate
FA	Fatty acids
FAM	Fatty acid medium
FBP	Fructose-1.6-bisphosphate
FBS	Fetal bovine serum
FGF	Fibroblast growth factors
FUM	Fumarate
G6P	Glucose-6-phosphate
GAL	Galactose
GAP	Glyceraldehyde 3-phosphate
GC-MS	Gas chromatography–mass spectrometry
GDH	Glutamate dehydrogenase
GFAM	Galactose and fatty acid medium
GLC	Glucose
GLCM	Glucose rich medium
GLN	Glutamine
GLU	Glutamate
GLUT	Glucose transporter
GPI	Glucose-6-phosphate isomerase

GSK3-β	Glycogen synthase kinase-3 beta
hESC	Human embryonic stem cells
hESC-CMs	Human embryonic stem cell derived cardiomyocytes
hiPSC	Human induced pluripotent stem cells
hiPSC-CMs	Human induced pluripotent stem cell derived cardiomyocytes
HIS	Histidine
HPLC	High performance liquid chromatography
hPSC	Human pluripotent stem cells
hPSC-CMs	Human pluripotent stem cell derived cardiomyocytes
IDH	Isocitrate dehydrogenase
IgG	Immunoglobulin G
IgM	Immunoglobulin M
ILE	Isoleucine
IPA	Ingenuity pathway analysis
LAC	Lactate
LACM	Lactate medium
LDH	Lactate dehydrogenase
LEU	Leucine
LYS	Lysine
MAL	Malate
MET	Methionine
MFA	Metabolic flux analysis
MID	Mass isotopomer distributions
NCX	Sodium-calcium exchanger
NKX-2.5	NK2 homeobox 5
OA	Oleic acid
OAA	Oxaloacetate
P5P	Pentose-5-phosphate
PA	Palmitic acid
PBS	Phosphate-buffered saline
PC	Pyruvate carboxylase
PDH	Pyruvate dehydrogenase
PEP	Phosphoenolpyruvate
PFA	Paraformaldehyde
PHE	Phenylalanine
PPP	Pentose phosphate pathway
PRO	Proline
PYR	Pyruvate
qMet	Specific metabolic rate
RYR	Ryanodine receptor
S7P	Sedoheptulose-7-phosphate
SER	Serine
SERCA	Sarco/endoplasmic reticulum calcium atpase
SR	Sarcoplasmic reticulum

SSEA-4	Stage-specific embryonic antigen-4
sTnI	Slow skeletal muscle isoform of troponin I
SUC	Succinate
TALDO	Transaldolase
TCA	Citric acid cycle
TGF-β	Transcription growth factor β
THR	Threonine
TRA-1-60	Human embryonic carcinoma marker antigen
TYR	Tyrosine
VAL	Valine
WB	Washing buffer
WNT	Wingless-related integration site

1. Introduction

1.1. Stem cell-based therapies for cardiac repair

Despite the recent advances in medicine, cardiovascular diseases remain the leading cause of death worldwide[1] (Fig.1.1). Several cardiovascular diseases, like myocardial infarction, are associated with a massive and permanent loss of cardiomyocytes, a non-proliferative and terminally differentiated cell population[2,3]. The current pharmacological and interventional therapies are not suitable to amend the effects of this cell loss, mainly due to the limited regenerative capacity of the myocardium[3,4]. Even though a subpopulation of cardiac stem cells reside in the adult human heart, these are unable to assure a meaningful functional recovery, since their renewal rate is only 1% per year[5] and a myocardial infarction can lead to the loss of approximately one third of the cardiomyocyte population[3]. On the other hand, the proliferation and migration of fibroblasts to the injury site forms scar tissue with impaired contractile function that ultimately leads to the progression of cardiac damage[6]. Thus, the only current treatment able to address cardiomyocyte loss and fully restore cardiac function is heart transplantation, a procedure limited by the number of compatible organs donated[1].

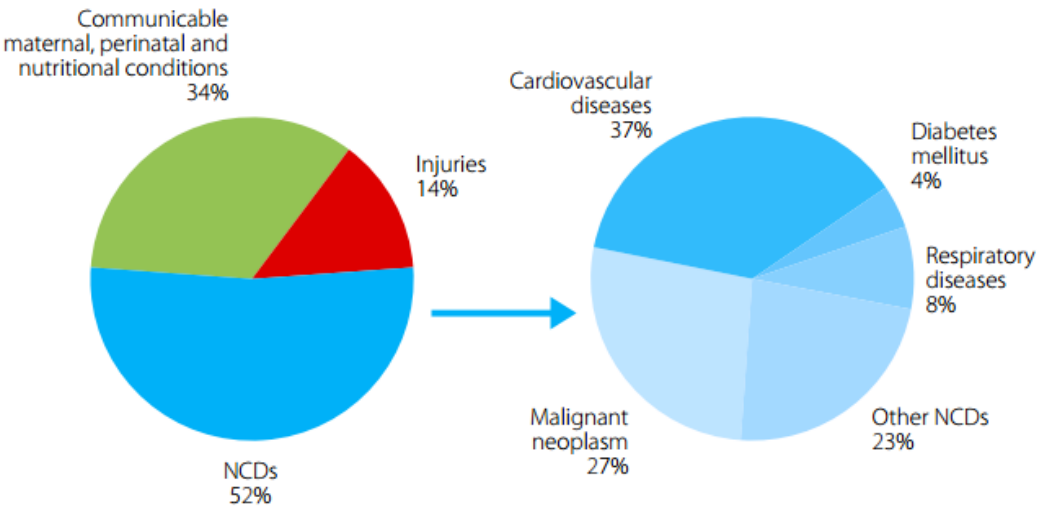

Figure 1.1 - Proportion of the leading causes of death worldwide. NCDs, noncommunicable diseases. Adapted from WHO, 2014[1].

Stem cell technology presents itself as a great promise in regenerative medicine, owing to stem cells ability to proliferate indefinitely, while maintaining an unspecialized state, and to differentiate into multiple cell lineages[7,8]. In fact, numerous groups have reported the use of different stem cells types, derived from different sources, to improve cardiac

function after injury[9-12]. Currently, the ESCORT[12] clinical trial (phase I) relies on the transplant of cardiac progenitors, derived from hESC embedded in a fibrin scaffold for the treatment of severe heart failure, leading to symptomatic improvements. Also no complications, such as arrhythmias, tumor formation or immunosuppression-related adverse events have been reported so far.

1.2. Human pluripotent stem cells

Stem cells can be divided into 3 categories, accordingly to their differentiation potential. Totipotent cells, corresponding to the zygote, are able to differentiate into all embryonic cells as well as extraembryonic tissues[13]. Pluripotent cells can differentiate into cells from all three germ layers, like human embryonic stem cells (hESC) that are obtained through isolation of the inner cell mass of blastocysts[7,8]. Finally, multipotent cells have the capacity to differentiate into cells from the same original lineage and can be found in several adult tissues such as bone marrow, muscle, brain, adipose tissue[13].

In 2006 a major breakthrough occurred in the stem cell field, as the reversion of somatic cells to a pluripotent state, by overexpression of Oct4, Sox2, Klf4 and c-Myc, was reported for the first time in mice[14]. This finding had such impact in the scientific community that the reprogramming of human induced pluripotent stem cells (hiPSC) derived from human dermal fibroblast was described shortly after the initial discovery in mice[15]. hiPSCs possess the same pluripotent properties as hESCs, surpassing the ethical concerns associated with the use of human embryos, therefore constituting an important alternative to hESCs in clinical applications. Furthermore, hiPSCs allow the implementation of an autologous therapy, as they can be derived from a patient's somatic cells, hence circumventing any concern of immune rejection[15].

hPSCs inherent capacity of unlimited self-renewal coupled with efficient directed differentiation protocols allow for the large-scale production of specific human cell types, which can be used in a wide range of applications, such as developmental biology[16], human disease modeling[17], drug screening[17] and regenerative medicine[18]. Even though animal models have been essential in research and clinical use, intrinsic differences with human biology limit the reliable use of these models. As such, hPSCs and their differentiated progeny hold great potential as a human cellular model[17].

1.3. Cardiomyocyte differentiation and enrichment

Differentiation of hPSCs to cardiomyocytes was first reported in 2001 and since then distinct approaches have been thoroughly explored, namely differentiation with cells cultivated as embryoid bodies[19] (three-dimensional aggregates of pluripotent stem cells), co-culture with inducer END-2 cells[20] and guided differentiation strategies (induced by growth factors and/or small molecules) in two dimensional monolayers[21]. Significant improvements in efficiency have been achieved through tightly timed, leveled and combined application of cardiogenic growth factors or small molecules to manipulate key developmental pathways like Wnt, TGF-β, Notch signaling, among others[21,22,23] (Fig. 1.2). Animal-derived growth factors are expensive and have several safety concerns associated, whereas chemically synthesized small molecules display greater stability and facilitated diffusion into multiple cell layers, thus decreasing variability and costs, making it the currently preferred methodology[21,22].

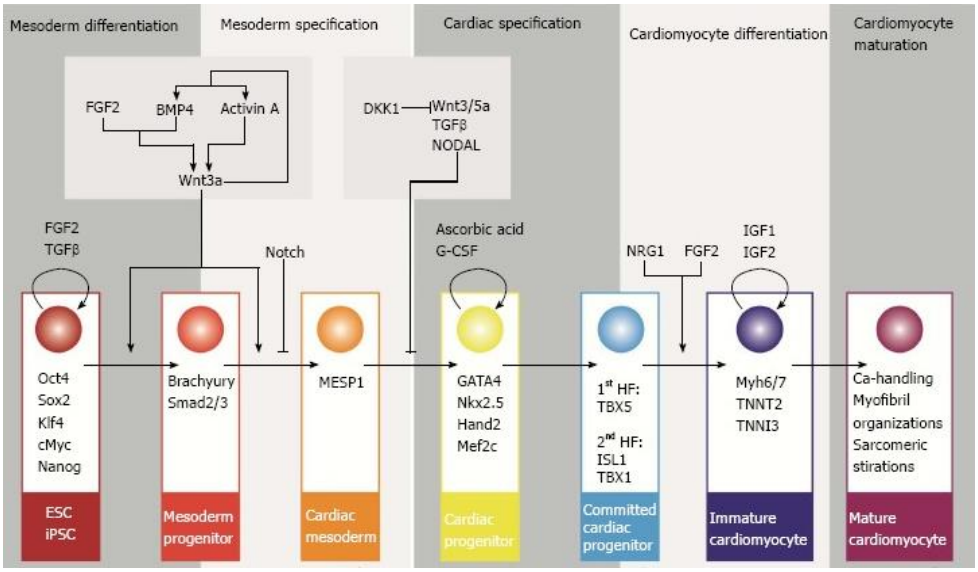

Figure 1.2 – Schematic representation of signaling pathways and factors involved in cardiomyocyte differentiation. Transcription factors associated with each cell type during cardiomyocyte differentiation are presented in the respective boxes. ESC: Embryonic stem cell; iPSC: Induced-pluripotent stem cells. Adapted from Kamps et al., 2016 [24].

Nowadays most protocols rely on the regulation of the Wnt pathway, which has a biphasic role in cardiogenesis, while initial Wnt activation is critical for mesoderm induction it then hinders cardiac specification[16]. Activation of Wnt pathway inhibits glycogen synthase kinase 3 beta (Gsk3-β) leading to accumulation of b-catenin that is translocated to the nucleus, where

it binds to transcription factors that regulate Wnt-responsive genes[16]. Hence, CHIR99021, a small molecule that inhibits Gsk3-β, has been widely used in directed differentiation protocols to activate Wnt signaling, whereas subsequent inhibition has been explored with a wide range of Wnt antagonist such as IWP4, IWP2, IWR1, Wnt-C59 or XAV939[21,23,25].

After differentiation, the purity of the final population of hPSC-derived cardiomyocytes (hPSC-CMs) is usually low. For example, the first methodology published in the literature yielded only 1-5% of beating cells[19]. Addition of growth factors and adaptation to monolayer-based directed differentiation techniques enhanced the yield to >30%[18], however this approach still presents significant variability between cell lines and experiments[26]. Temporal modulation of Wnt signaling has shown great progress towards the generation of hPSC-CMs, with high purity (80-98% of cTnT-expressing cardiomyocytes), obtained from both hESC and hiPSC lines[21].

The persistence of undifferentiated hPSC is a great safety concern for clinical applications, as the tumorigenic potential of hPSC may lead to the formation of malignant tumors when transplanted into the host[27]. Thus, throughout the years several strategies have been explored to remove these cell contaminants and improve the purity of hPSC-CMs. For instance, the use of Percoll gradients[28], Flow Activated Cell Sorting for specific surface markers[29] and for cells incubated with mitochondrial dyes[30] or molecular beacons[31] have already been reported. One elegant and more efficient approach is to culture hPSC-CM in medium containing lactate (LAC) instead of glucose (GLC)[32]. Since hPSC and fibroblasts rely highly on glucose, only cardiomyocytes, which can use both metabolites, survive when cultured in this medium[32].

1.4. Maturation of hPSC-CMs

Notwithstanding the progress made in improving differentiation protocols, the final population of hPSC-CM obtained remains immature with a fetal-like phenotype, whether in terms of structure[33], gene expression[34], metabolism[35], contractile function or electrophysiology[36] (Table 1.1). Thus, immaturity is currently a critical obstacle hampering the potential of hPSC-CMs in cell therapy, drug discovery, toxicity testing and cardiac disease modeling[37].

A wide range of strategies to improve maturation of hPSC-CM have been explored so far. These include the overexpression of microRNAs that regulate cardiac development[38]; addition of chemical supplements to the culture medium, like the growth hormone T3[39]; and

culture of hPSC-CMs in organic or synthetic scaffolds coupled with cyclic stretching[40] and/or electrical cues[41], which have been reported to improve the expression of cardiac markers, cell morphology and ultrastructure, respiratory capacity and contractile kinetics. Nonetheless a mature phenotype reminiscent of fully recapitulated adult cardiomyocytes has yet to be achieved.

Table 1.1 – **Comparison of hPSC-CM and adult human cardiomyocytes.** Adapted from White et al., 2016 [37].

		Human PSC-CMs	Adult human CMs
Morphology	Shape	Circular (isotropic)	Rod shaped (anisotropic)
	Length-width ratio	Irregular	7:1 to 9.5:1
Ultrastructure	Nuclei	Mono-nuclear	Bi- or Multi-nuclear
	Mitochondria	Small fraction	20-40% of cell volume
	T-tubules	Absent	Present
	Sarcomere	1.65 μm	2.2 μm, highly organized
Electrophysiology	Beats per minute (bpm)	40 bpm	60–100 bpm
	Upstroke velocity, dV/dtmax or Vmax	10–150 V/s	300 V/s
	Resting membrane potential	−30 to −75 mV	−85 to −95 mV
	Conduction velocity	0.1 m/s	0.3–1.0 m/s
Metabolic Profile	Energy substrate/pathway	Glucose/glycolysis	Fatty acid/β-oxidation

1.5. Cardiomyocyte structure and contraction

Adult cardiomyocytes have an elongated rod-like shape and present a highly organized internal structure composed of numerous parallel myofibrils, which consist of longitudinal repetitions of sarcomeres, the functional units of muscle[42]. Cardiomyocyte shape and sarcomere alignment have functional implications in excitation-contraction coupling and in the generation of contractile force[43]. During pathogenic hypertrophy cardiomyocytes adopt a rounder shape and display disorganized sarcomeres[44], as such pathogenic growth has been reported to accompany several forms of heart disease[45]. In contrast, physiological hypertrophy, which occurs during normal heart development, the addition of new sarcomeric units is in longitudinal series or parallel to pre-existing ones thus maintaining sarcomere alignment and cardiomyocyte shape[44].

The sarcomere is composed of a complex assembly of both thick and thin filaments, the former consists of myosin while the latter includes actin, troponin and tropomyosin. Each sarcomere is delimited at either end by a Z-disc, which is included in the I-band, composed by thin filaments that extend in both directions (Fig. 1.3). The A-band comprises the portion of the sarcomere where thick and thin filaments overlay, while the H-zone in the center of the A-band contains only thick filaments. In the middle of the H-zone is the M-line that corresponds to the center of the sarcomere[46].

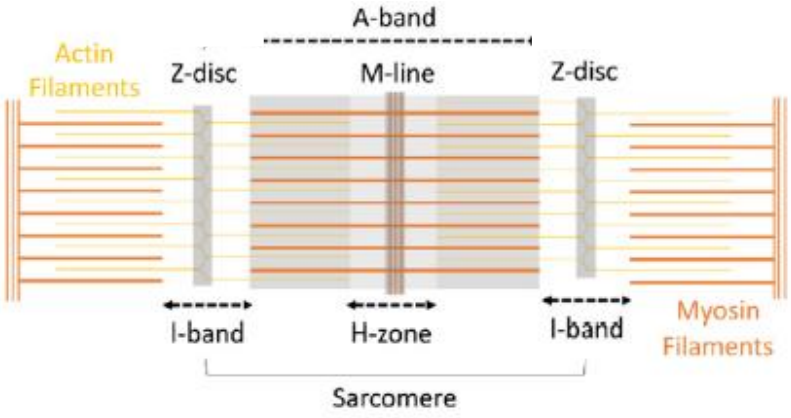

Figure 1.3 – Schematic representation of the ultrastructural features of sarcomeres. Adapted from Feric et al., 2015[47].

During an action potential of adult cardiomyocytes, membrane depolarization activates voltage gated calcium (Ca^{2+}) channels allowing the entry of Ca^{2+} into the cell. This triggers the release of Ca^{2+} from the sarcoplasmic reticulum in a positive feedback process, the Ca^{2+}-induced-Ca^{2+} release[48]. The binding of Ca^{2+} to troponin induces a conformational change and displaces tropomyosin, thereby exposing the binding sites of actin to which energized myosin heads will attach forming cross-bridges[49] (Fig. 1.4). Consequent release of ADP and P_i (inorganic phosphate) bend the myosin heads, which switch to a low energy state, pulling the actin filaments toward the center of the sarcomere (M-line). Binding of ATP to the myosin heads lead to cross-bridge detachment, and ATP hydrolysis restores myosin to the energized state and raised conformation. Since thin filaments are anchored to the Z-discs, this process leads to sarcomere shortening, thus resulting in cell contraction[46]. During relaxation, Ca^{2+} is pumped back into the sarcoplasmic reticulum and to a lesser degree extruded from the cell, so as to return the cell to resting Ca^{2+} levels. As Ca^{2+} detaches from troponin, this protein returns to the initial conformation simultaneously moving tropomyosin to cover the actin binding sites. This blocks myosin from forming cross-bridges, therefore a new cycle of contraction is only possible after a new stimuli[48].

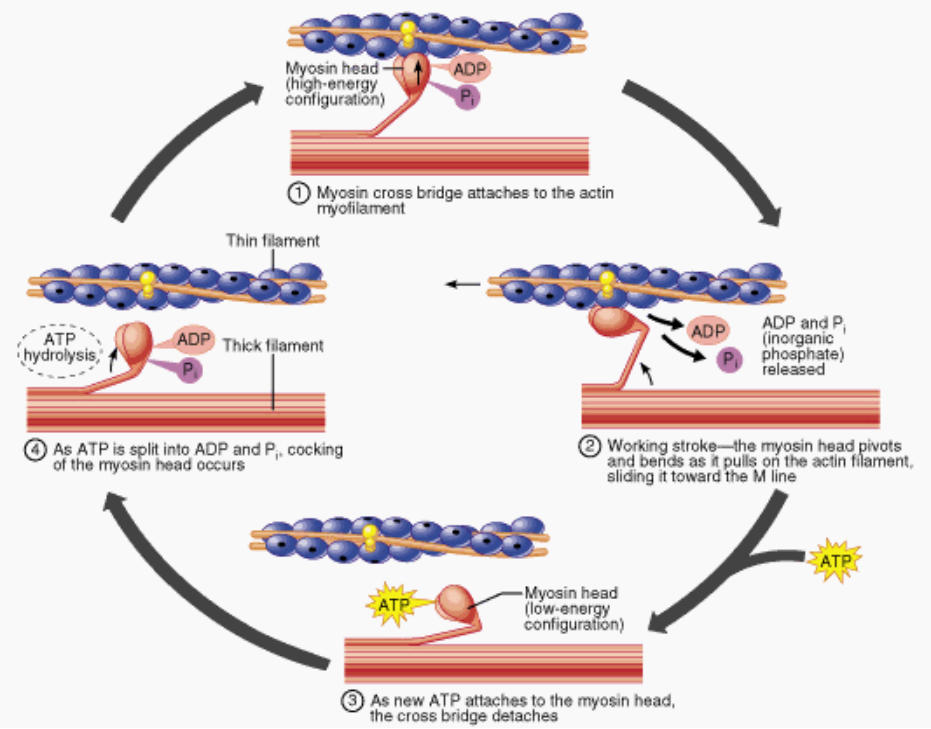

Figure 1.4 – Schematic representation of the cross-bridge cycle. Adapted from Martini et al., 2011[50].

1.6. Metabolic dynamics during heart development

The incessant contractile function of the human heart, along with cardiomyocytes minimal ability to store high-energy phosphates, results in a high metabolic demand requiring a continuous high production rate of ATP to sustain proper cell function[35,51]. However, the metabolic profile of the fetal heart is not compliant with this demand, since at this point of development cardiomyocytes are highly dependent on glycolysis, and to a lesser extent lactate oxidation, to produce ATP[35]. Hence, during heart development, a metabolic shift occurs from primarily glycolytic to an oxidative metabolism, where the adult heart relies mainly on mitochondrial fatty acids (FA) oxidation to ensure ATP production[35]. Nevertheless, cardiomyocytes retain metabolic plasticity to use other substrates (glucose, lactate, amino acids, ketone), depending on their availability[35,52].

In vitro, hPSC-CMs rely mainly on glycolysis when cultured in media containing glucose, even if present at low concentrations in media with other substrates available[32,53]. In the absence of glucose, hPSC-CMs were able to metabolize other substrates to support cell function[32,53]. Notably, galactose (GAL) alone or in combination with fatty acids was able to induce the metabolic switch in hiPSC-CMs, as well as an increase in mitochondrial reserve and maximum respiratory capacity[53]. Even so, a link between the metabolic shift and maturation of hPSC-CM *in vitro* has not been established.

1.7. Metabolic Flux Analysis

Metabolic flux analysis (MFA) is currently the preferred technique to obtain quantitative data about *in vivo* metabolism[54]. Initially, MFA studies relied on metabolite balances within an assumed network stoichiometry, where external rate measurements provided constraints to determine intracellular fluxes. However this approach could not distinguish fluxes of parallel pathways (e.g. glycolysis vs. pentose phosphate pathway), reversible reactions, and cyclic pathways. A shortcoming overcome by combining MFA with measurement of the metabolic conversion of stable isotopic tracers, like ^{13}C, by mass spectrometry or nuclear magnetic resonance[55]. Thus, providing additional independent constraints for flux estimation greatly improving quantitative resolution of metabolic flux distributions, at the expense of increased experimental and computational complexity. Currently, the elementary metabolic unit (EMU) method is considered the most advanced and efficient computational approach for simulating isotopic labeling distributions[56].

In summary, nonstationary ^{13}C-MFA relies on computational simulation to estimate a set of feasible intracellular metabolic fluxes that minimize the variance-weighted sum of squared residuals between the predicted and measured transient ^{13}C-labeling data and extracellular rate measurements[54].

Despite the increasing role of nonstationary ^{13}C-MFA in metabolism studies of a wide range of biological systems[54,57,58], a metabolic network model of hiPSC-CMs has yet to be explored.

2. Aim of the thesis

The main aim of this thesis was to evaluate if altering the composition of hPSC-CM culture medium to mimic substrate availability during cardiac development, would promote hPSC-CMs maturation *in vitro.*

Based on a recently developed methodology for the directed differentiation of hPSC into cardiomyocytes in two dimensional monolayer culture systems, the first objective of this thesis was to perform a proteomic characterization of two distinct cell populations: pluripotent stem cells (hPSC) and cardiomyocytes (hPSC-CM).

After differentiation, hiPSC-CMs were cultured in glucose depleted medium supplemented with either i) fatty acids (FAM), ii) galactose and fatty acids (GFAM) or iii) lactate during the first 10 days followed by a switch to galactose and fatty acids (LACM&GFAM), using the standard glucose rich hiPSC-CMs medium (GLCM) as reference (Fig. 2.1). To study the impact of distinct carbon sources in metabolic profile and maturation status of hiPSC-CMs, metabolomics methodologies such as HPLC and GC-MS were used and structural analysis was performed throughout 20 days of culture. Additionally, parallel labeling experiments and ^{13}C-MFA were used for estimation of intracellular flux distributions (fluxome).

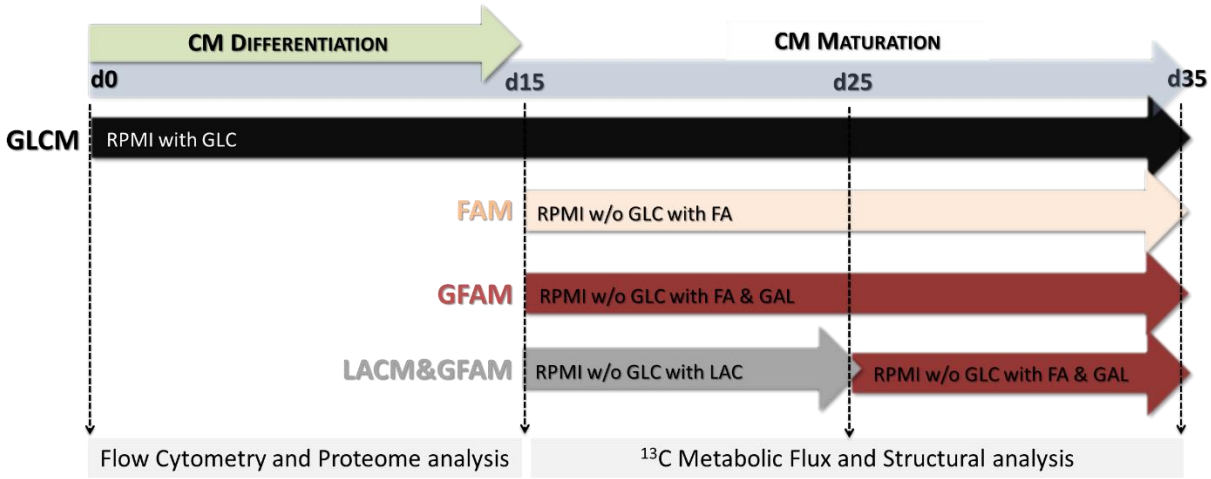

Figure 2.1 – Schematic representation of the strategies and procedures performed to achieve the aims of the thesis.

3. Materials and Methods

3.1. Cell Culture

3.1.1. hPSC maintenance and differentiation to cardiomyocytes

In this study two hPSC cell lines were used, the hiPSC line DF19-9-11T.H from WiCell as well as the cardiac fluorescent reporter cell line hESC-NKX2.5(eGFP/w)[59] kindly provided by Dr. David Elliot (Murdoch Children Research Institute). In this reporter line, eGFP was targeted to the genomic locus of the cardiac transcription factor NKX2.5, therefore being expressed upon differentiation towards the cardiac lineage, with further increase in functional cardiomyocytes[59]. hPSCs were cultured on Matrigel® (Corning) coated plates in mTESR1 medium (STEMCELL Technologies) until reaching 80%-90% confluency at which point differentiation to cardiomyocytes was induced as previously described[60]. Briefly, this directed differentiation protocol involves the use of RPMI+B27 medium (Invitrogen) and serial application of Activin A (PeproTech), CHIR99021 (Biogen Cientifica S.L.), Ascorbic Acid (Sigma-Aldrich) and IWR1 (Sigma-Aldrich) in bidimensional monolayer culture conditions. Cells were cultured at 37°C, in a humidified atmosphere of 5% CO2.

3.1.2. hiPSC-CM maturation

After 15 days of differentiation, hiPSC-CMs were cultured for further 20 days in four different culture media formulations (Fig. 2.1): i) GLCM (Glucose Medium): standard hiPSC-CM medium (RPMI+B27); ii) FAM (Fatty Acid Medium): RPMI without GLC supplemented with B27, 1mM glutamine (GLN) (Alfagene), 100µM oleic acid (OA), 50µM palmitic acid (PA) (both from Sigma-Aldrich); iii) GFAM (Galactose and Fatty Acid Medium): RPMI without GLC supplemented with B27, 1mM GLN, 10mM galactose (Sigma-Aldrich), 100µM OA and 50µM PA; and iv) LACM&GFAM: 10 days in RPMI without GLC supplemented with B27, 1mM GLN and 4mM sodium L-lactate (Sigma-Aldrich) (Lactate Medium) and another 10 days in GFAM (Figure 1A). At day 25 (d25) and 35 (d35), hiPSC-CMs were collected for metabolic and structural analysis.

3.1.3. Cell concentration and viability

Cell concentration and viability were determined by cell counting in a Fuchs–Rosenthal haemocytometer (Brand) using the trypan blue (Sigma-Aldrich) exclusion method (0.1% (v/v) in PBS).

3.2. Characterization of hPSC-CMs

3.2.1. Flow cytometry analysis

Cells were dissociated with TrypLE^{TM}Select (Invitrogen) and ressuspended in washing buffer (WB) solution (5% (v/v) FBS in PBS). After two washing steps with WB, cells were incubated with primary antibody for 1 h at 4°C followed by another set of 2 washing steps with WB. For determination of intracellular markers the BD Cytofix/Cytoperm™ kit (BD Biosciences) was used accordingly to the manufacturer's instructions. Cells were incubated with secondary antibody for 30 min at 4°C. Finally, cells were suspended in WB and analyzed in a flow cytometer (CyFlow® space, Partec GmbH) registering at least ten thousand events per analysis. Primary antibodies used: Tra-1-60, SSEA-4, isotype control antibodies (1:10, all Santa Cruz Biotechnology) and cardiac Troponin T (cTnT) (1:20, Thermoscientific). Secondary antibodies used were: goat anti-mouse IgM-AlexaFluor488 and goat anti-mouse IgG-AlexaFluor488 (1:200, all from Invitrogen)

3.2.2. Qualitative total proteome analysis

Cell pellets from d0 and d15 of differentiation from both cell lines were lysed in 50mM Tris, 5mM EDTA, 150mM NaCl, 1% Triton X-100 (all from Sigma-Aldrich) and 1X Protease Inhibitor (Roche), for 45 minutes at 4ºC. Centrifuged at 15000g for 15 minutes at 4ºC and collected the supernatant. Protein concentration was assessed by microBCA (Thermoscientific) following manufacturer's instructions. Normalized quantities of protein were reduced, alkylated and digested overnight at 37 ^{0}C with trypsin (Promega, 1.6 ng/µl). The digested samples were lyophilized using a SpeedVac centrifuge (ThermoSavant) and dissolved in 12 µl of water with 0.1% formic acid. An Eksigent LC 4500 coupled to TripleTOF 6600 (Sciex) equipment was used to analyze the samples. Two biological replicates per time point were run in technical triplicate. Data was acquired with the Analyst software TF 1.7 (Sciex) and analyzed using the ProteinPilot software (Sciex). The complete data set of proteins identified was further analyzed with Ingenuity Pathway Analysis (IPA) software (Qiagen)[61]. Statistically significant over-representation of given biological functions and canonical pathways were identified based on a probability score, p-value. This p-value is calculated by considering the total number of proteins know to be associated with a determined function or pathway, and their representation in the selected dataset. IPA's calculated score was displayed as the negative log of p-value.

3.3. Nonstationary ^{13}C-Metabolic Flux Analysis

3.3.1. Metabolite analysis

Glutamine (GLN), glutamate (GLU), glucose (GLC) and lactate (LAC) concentrations from culture supernatants were measured using YSI 7100MBS (YSI Incorporated). Enzymatic assay kits were used to quantify ammonia (NZYTech), galactose and fatty acids (both from Abcam). Amino acid concentration was determined by HPLC using the Waters AcQ.Tag Amino Acid Analysis Method (Waters), as described elsewhere[62]. The specific metabolic rates (qMet, expressed in $\mu mol.h^{-1}.10^6\ cell^{-1}$) were calculated using the equation: $qMet = \Delta Met/(\Delta t \times Xv)$, where ΔMet (mol/L) is the variation of metabolite concentration during the time period Δt (h), and Xv (cell/L) the average of cell concentration during the same time period.

3.3.2. Isotopic tracer experiments and GC-MS analysis

For the parallel isotopic labelling experiments the following isotopic tracers were used: [1,2-^{13}C]Glucose; [U-^{13}C]Glutamine; [3-^{13}C]Sodium L-Lactate; [U-^{13}C]D-Galactose (all from Cambridge Isotope Laboratories) and [18-^{13}C]Oleic Acid; [16-^{13}C]Palmitic Acid (from Sigma-Aldrich). Only one isotopic tracer was used at a time to allow monitoring of the incorporation of each tracer. Label incorporation was characterized 24 and 48h after label addition. At the chosen time points, culture supernatants were collected and each plate was completely dipped in liquid N_2. After addition of 1mL of 50% (v/v) ice-cold acetonitrile (ThermoFisher) to each well, cells were scrapped and collected. Cell extracts were centrifuged at 15000 g for 10 min at 4°C, and collected supernatants were lyophilized overnight using a SpeedVac centrifuge (ThermoSavant). Amino acids, lactate and TCA intermediates were derivatized with N-methyl-N-tert-butyldimethylsilyl-trifluoroacetamine (MBDSTFA, Aldric, DE) as reported elsewhere[58].

Metabolites were analyzed in a QP2010 mass spectrometer (Shimadzu, Japan) in the EI mode (70 eV) with a HP-5 MS column (Agilent Technologies). The obtained spectra were analyzed and integrated using GC-MS Solution software version 2.50 SU1 (Shimadzu, Japan). Mass Isotopomer Distributions (MID) were calculated after spectra integration and corrected for natural isotope abundance. The contribution of each ^{13}C-labeled substrate to TCA cycle intermediates was determined as the percentage of tracer incorporation in citrate, fumarate and malate.

3.3.3. Metabolic network and nonstationary ^{13}C-MFA

Nonstationary ^{13}C-MFA of parallel labelling experiments was performed using the software package INCA[63], which automatically generates and simulates mass and material balance equations from a user-defined metabolic network structure and experimental datasets. At least 10 restarts with random initial values for the parameters (intracellular fluxes and pools) were performed to find a global optimum.

3.3.4. ATP production

ATP production was estimated by taking into account referenced ATP production in glycolysis, TCA and b-oxidation by each substrate[64] and respective flux values determined in nonstationary ^{13}C-MFA.

3.4. Assessment of hiPSC-CM structure

3.4.1. Immunofluorescence microscopy

Cells were washed with DPBS and fixed in 4% (w/v) PFA in DPBS solution for 15 min. After being permeabilized and blocked with 5% (v/v) FBS, 1% (w/v) BSA, 0.3% (v/v) Triton X-100 in DPBS for 1h, at room temperature (20-25°C), cells were incubated with primary antibody, troponin I (1:100, Millipore), diluted in 1% (w/v) BSA, 0.1% (w/v) TX-100 in PBS overnight at 4°C. Afterwards, cells were washed in DPBS and incubated with secondary antibody, Alexa Fluor 594 goat anti-mouse IgG (1:500, Invitrogen), in the dark for 1h at room temperature (20-25°C). Cell nuclei were counterstained with Hoechst 33342 nucleic acid dye (1:1000, Thermo Scientific). Representative images were taken using an inverted fluorescence microscope (DMI 6000, Leica).

3.4.2. Cell morphology

Cell area, circularity index and aspect ratio were determined in ImageJ software (National Institutes of Health) using standard analysis plugins. For each condition, at least 70 cells were evaluated.

3.4.3. Measurement of mitochondrial membrane potential

Differences in mitochondrial membrane potential, were evaluated using Mitoview™ 633 (Biotium) following manufacturer's instructions. Briefly, after incubation with the dye for

1 h, fluorescence was measured in a microwell plate fluorescence reader, Infinite 200 PRO NanoQuant (TECAN).

3.4.4. Lipid droplets content

Lipid droplet content was assessed using the Lipid Droplets Fluorescence Assay Kit (Cayman), according to the manufacturer's instructions. Fluorescence was quantified in a microwell plate reader, Infinite 200 PRO NanoQuant (TECAN).

3.5. Statistical analysis

Statistical analysis was performed using GraphPad Prism Software version 5 (GraphPad Software). Values are represented as mean±SD of independent measurements or assays (at least n=3 replicates were considered). Statistical significance was evaluated using Student's t test with Welch's correction. Values of $p<0.05$ were considered statistically significant.

4. Results and Discussion

4.1. hPSC-CMs remain highly glycolytic regardless of metabolic development during differentiation

Starting with a protocol previously implemented in the lab for the directed differentiation of hPSC-CMs in two dimensional monolayers[60], cells' proteome characterization was pursued through mass spectrometry tools. Two hPSC lines were used: 1 hiPSC line (DF19-9-11T.H) and 1 hESC line (cardiac fluorescent reporter cell line hESC-NKX2.5(eGFP/w))[59].

Cell population was characterized by flow cytometry before (hPSC, d0) and 15 days after inducing cardiomyocyte differentiation (hPSC-CM, d15). At d0, pluripotency markers SSEA4 and TRA-1-60 were highly expressed (>90%) in both hiPSC and hESC lines, confirming the maintenance of pluripotency throughout cell expansion in monolayer culture (Fig. 4.1 A). The efficiency of cardiomyocyte differentiation was evaluated by analyzing the percentage of cTnT and eGFP-expressing cells in hiPSC and hESC, respectively, at d15. Results showed that 94.0±4.7% and 85.7±5.5% of cTnT and eGFP-expressing cells in hiPSC and hESC, respectively, were attained (Fig. 4.1 B and C), which confirms the high efficiency of temporal modulation of Wnt signaling in directing cardiomyocyte differentiation from both hESC and hiPSC lines[21]. Furthermore, hPSC-CMs start displaying spontaneous contraction at day 6 of differentiation, maintaining this automaticity throughout culture time.

Cell pellets were collected from hPSC populations at both time points (d0 and d15) for qualitative total proteome analysis. From the total proteins identified, 40-50% are exclusive to either hPSC (d0) or hPSC-CM (d15) (Fig. 4.1 D and E), revealing an extended degree of variation in the proteome profile during differentiation to a cardiac lineage. Total proteome data was analyzed with IPA for predictive insights of biological functions and canonical pathways relevant for each sample time point. This software analyzes large datasets to find the most significant functions and pathways based on a calculated probability score, attributing a p-value to each annotation[61]. Analysis of the proteomic profile identified two clearly distinct cell populations, in this case hPSC and hPSC-CMs. In hPSC there is a significant over-representation of proteins associated with proliferation and cell cycle (Fig. 4.1 F), which were not observed in hPSC-CMs. Even though previous reports have termed cardiomyocytes as non-proliferative cells, by measurement of the chemiluminescence of BrdU (5-bromo-2′-deoxyuridine) incorporation during DNA synthesis[4], this data

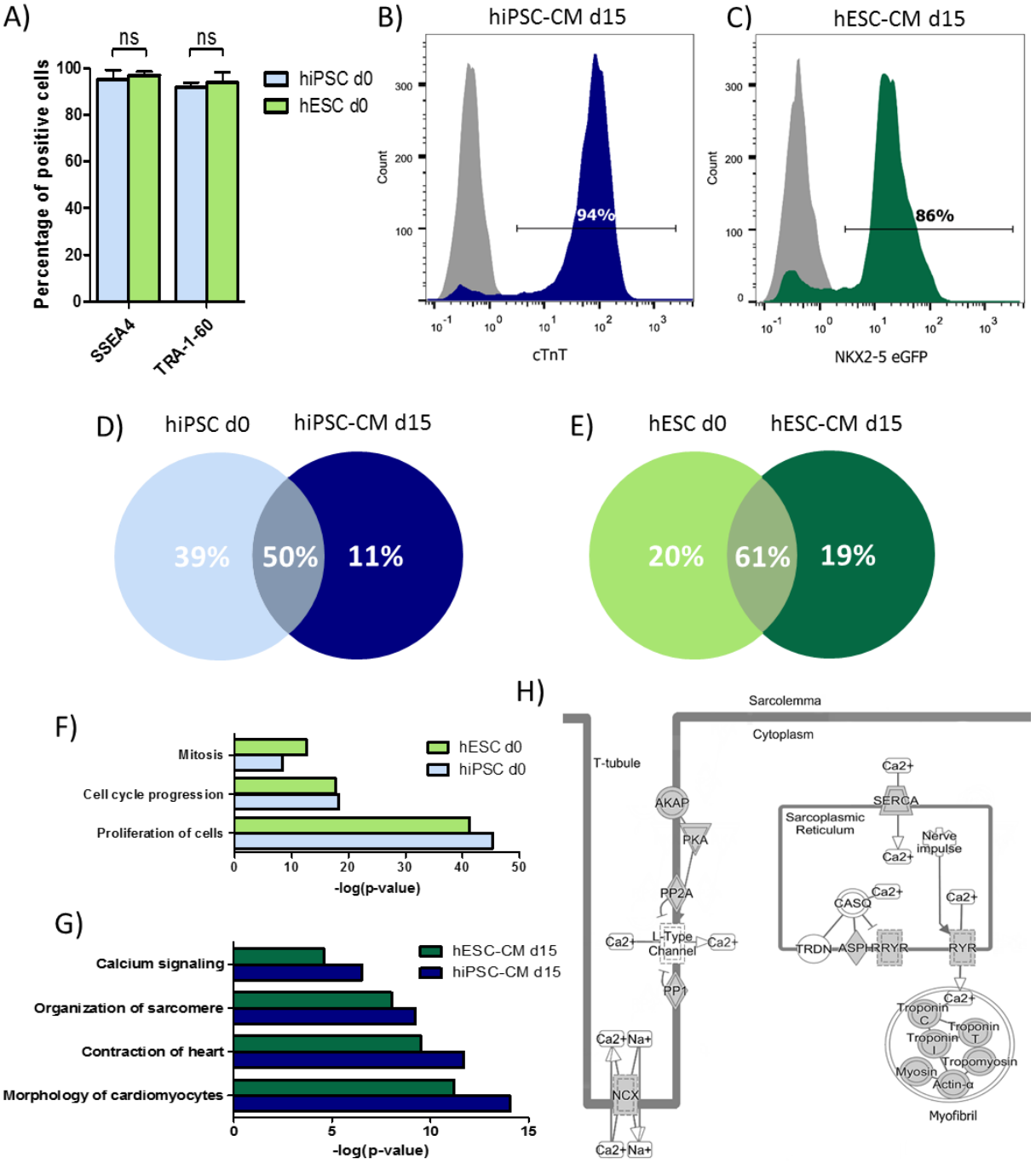

Figure 4.1 – hPSC-CMs exhibit cardiac specific markers after 15 days of differentiation. Percentage of positive cells expressing: pluripotency markers at d0 (**A**) and cardiac markers at d15 (**B**) and (**C**); was assessed by flow cytometry. Typical $cTnT^{+}$ and $Nkx2.5\text{-}eGFP^{+}$ populations in cells produced from the applied differentiation protocol are represented in (**B**) and (**C**), respectively. Grey histograms represent isotype control. Venn diagram illustrating the overlap of all proteins identified by qualitative proteome analysis, at d0 and d15 in (**D**) hiPSC and (**E**) hESC. Enrichment in biological functions determined with IPA at (**F**) d0 and (**G**) d15. IPA's calculated score is displayed as the negative log of p-value, the cut-off considered is 1.3. (**H**) Schematic representation of the link between calcium signaling and muscle contraction at d15, adapted from IPA. Grey depicts proteins present in the selected dataset whereas in white are proteins involved in these processes but not present in the data. Data represented as mean±SD. ns, not significant.

demonstrates that the difference in the proliferative phenotype of pluripotent stem cells and cardiomyocytes is evident even at the proteome level. After 15 days of differentiation there is an enrichment of cardiac related biological functions, specifically cardiomyocyte morphology, sarcomere organization, contraction and calcium signaling pathway (Fig. 4.1 G), further reinforcing the data obtained from flow cytometry (Fig. 4.1 B and C) and the assumption that the methodology applied was successful in directing the differentiation of both hiPSC and hESC into cardiomyocytes.

A closer look into the proteins identified that are involved in the calcium signaling pathway revealed the presence of the main calcium channels that regulate muscle contraction in cell populations from d15 (Fig. 4.1 H). For example: RYR, ryanodine receptor that upon depolarization releases Ca^{2+} from the sarcoplasmic reticulum (SR), inducing muscle contraction[65]; SERCA the sarco/endoplasmic reticulum calcium ATPase that actively transports Ca^{2+} from the cytoplasm into the SR[65]; and NCX, the Na^{+}-Ca^{2+} exchanger that during relaxation prevents overloading of intracellular stores by exporting Ca^{2+} from the cell[66]. Moreover, all of the myofilaments essential for cardiac contraction were present in proteomics data from both cell lines at d15 (Fig. 4.1 H). Troponin is a heterotrimeric protein complex composed of troponin-I, troponin-T and troponin-C[49]. Binding of Ca^{2+} to the latter triggers a conformational shift in the complex formed by troponin and tropomyosin, exposing α-actin for interaction with myosin ultimately resulting in a contraction[49]. Also of note was the identification of cTnI, the adult cardiac isoform of troponin I, in both hPSC-CMs lines. After birth this adult isoform completely and irreversibly replaces the fetal isoform sTnI[67]. Although the sTnI isoform was still identified in hPSC-CMs, the identification of cTnI hints that the differentiation protocol applied was able to, at least in part, mimic heart development until this transitioning phase.

Proteomic analysis also revealed an overall enrichment in metabolic pathways in hPSC-CMs when compared to hPSC. A distinct over-representation of proteins related to oxidative phosphorylation, TCA cycle, glycolysis and fatty acid β-oxidation pathways was observed in hPSC-CMs (Fig. 4.2 A). While these results may allude to an increased oxidative metabolism, that is not the case seeing as metabolic results suggest that both hPSC and hPSC-CMs rely mainly on anaerobic glycolysis[32]. Analysis of the ratio between lactate production and glucose consumption confirms maintenance of the glycolytic profile in both cell populations ($Y_{LAC/GLC}$=1.74 in hPSC vs 1.76 in hPSC-CMs) (Fig. 4.2 B). In anaerobic glycolysis, glucose is channeled for lactate production, thus this ratio theoretically equals 2 [64]. A pondered evaluation of both proteomics and metabolite data suggests that although hPSC-

CMs remain highly glycolytic, the increased identification of proteins involved in oxidative metabolic pathways after 15 days of differentiation reflects an overall development in terms of metabolic machinery during cardiomyocyte differentiation. This suggests a relation between hPSC-CMs metabolic profile and the carbon source available in the medium. Therefore further metabolic studies were pursued to investigate this possible link, using only the hiPSC cell line.

Overall, resource to mass spectrometry tools allowed for a proteomic characterization of both hPSC and the final population of hPSC-CMs obtained, revealing an enrichment in cardiac markers and metabolic machinery in hPSC-CMs. Therefore this tool revealed itself valuable in complementing other analytical tools widely reported in the literature to characterize hPSC-CMs[21-23]. A drawback of the methodology applied herein lies with the fact that this proteome analysis is not quantitative. This limits additional conclusions particularly from the set of proteins present in both hPSC and hPSC-CMs, since a quantitative analysis could expose differences in proteins up- or down-regulated. To surpass this limitation a quantitative approach, like SWATH[68], could be used in future proteome analysis to elucidate the evolution of the proteomic profile throughout the directed differentiation of hPSC-CMs.

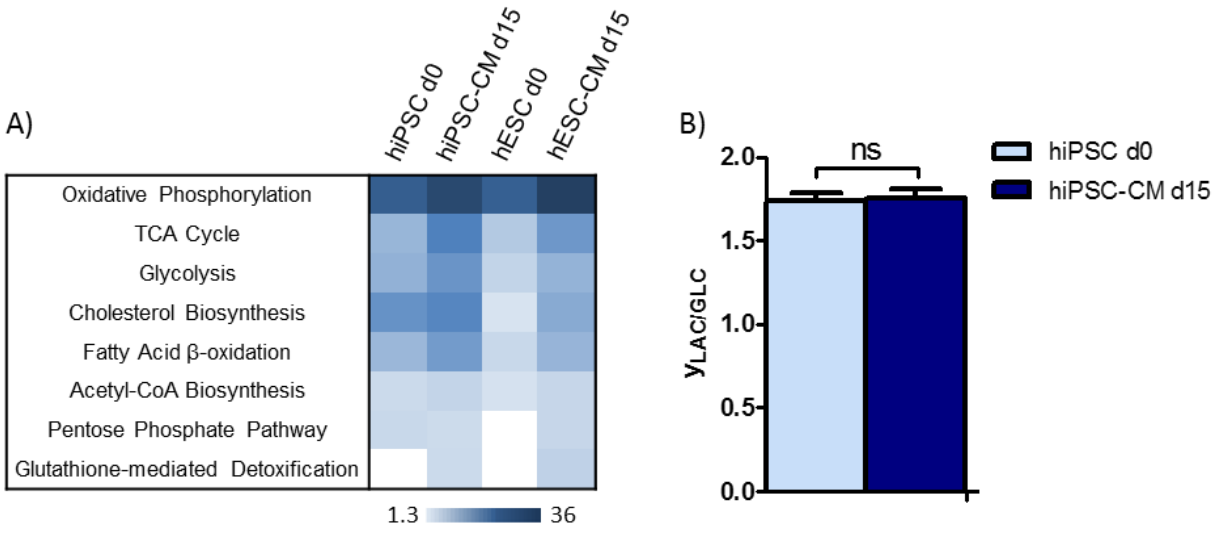

Figure 4.2 – hPSC-CMs remain highly glycolytic despite development of metabolic machinery during differentiation. (**A**) Heatmap depicting top metabolic canonical pathways determined by IPA, the calculated score is displayed as the negative log of p-value, and the cut-off considered is 1.3. (**B**) Ratio between lactate production and glucose consumption, $y_{LAC/GLC}$. Data represented as mean±SD. ns, not significant.

4.2. hiPSC-CMs shift to an oxidative metabolism in the absence of glucose

After 15 days of differentiation, hiPSC-CMs were maintained for an additional 20 days (i.e. from day 15 to 35) in distinct glucose depleted culture media besides the standard glucose rich medium used as reference, as described above (section 2, Fig. 2.1). Samples were collected at day 15, 25 and 35 (hereafter designated as d15, d25, d35) of total culture time (Fig. 2.1). Analysis of the metabolic profile of the main substrates available in each media throughout culture, confirms that hiPSC-CMs maintained in glucose rich medium (GLCM) remain highly dependent on anaerobic glycolysis, as denoted by the high production rate of lactate at d35 (Fig. 4.3 A). However, in the absence of glucose, hiPSC-CMs were able to metabolize other substrates namely lactate, fatty acids and galactose (Fig. 4.3A), showing remarkable metabolic plasticity as previously described for human adult cardiomyocytes[35]. Furthermore, a shift occurs from a metabolism highly dependent on anaerobic glycolysis, since there is no production of lactate in either FAM, GFAM or LACM&GFAM media. Hence, the overall development of metabolic machinery during differentiation, revealed by proteomics analysis (Fig. 4.2), may reflect a developmental adaptation of hiPSC-CMs to the consumption of distinct carbon sources and consequent metabolization through oxidative pathways. Additionally, these results suggest that when the main substrate available in the media is glucose, the preferred consumption of this substrate[53] restricts hiPSC-CMs metabolism to a glycolytic profile.

Culture of hiPSC-CMs with uniformly ^{13}C-labelled versions of the corresponding substrates allowed the analysis of the incorporation of ^{13}C into lactate and TCA cycle intermediates (citrate, fumarate and malate). hiPSC-CMs maintained in GLCM showed no improvements in oxidative capacity from d15 to d35, seeing as around 90% of lactate derived from [1,2-^{13}C]Glc, upon 48h incubation, and the fraction of intracellular pools of TCA cycle intermediates remained unchanged (Fig. 4.3 B).

At d15 the switch to FAM showed that although the switch to reliance on fatty acid metabolization was immediate, it occurred in a low degree with only 18% of the labeled fraction of TCA cycle intermediates deriving from [U-^{13}C]PA and [U-^{13}C]OA at d15 (Fig. 4.3 C). The remaining 82% derived from [U-^{13}C]Gln, which suggests an important contribution of glutaminolysis to support TCA cycle anaplerosis. However, at d25 the contribution from fatty acids to TCA cycle increased to 35%, revealing an adaptation to fatty acid consumption. In the presence of galactose (GFAM), the incorporation of [U-^{13}C]Gln decreased to 38%, in favor of [U-^{13}C]Gal incorporation in TCA cycle (Fig. 4.3 D). Moreover hiPSC-CMs showed

an adaptation to fatty acid consumption similar to that observed in FAM, as the overall contribution to labeled TCA cycle pools increased from 19% at d15 to 36% at d35.

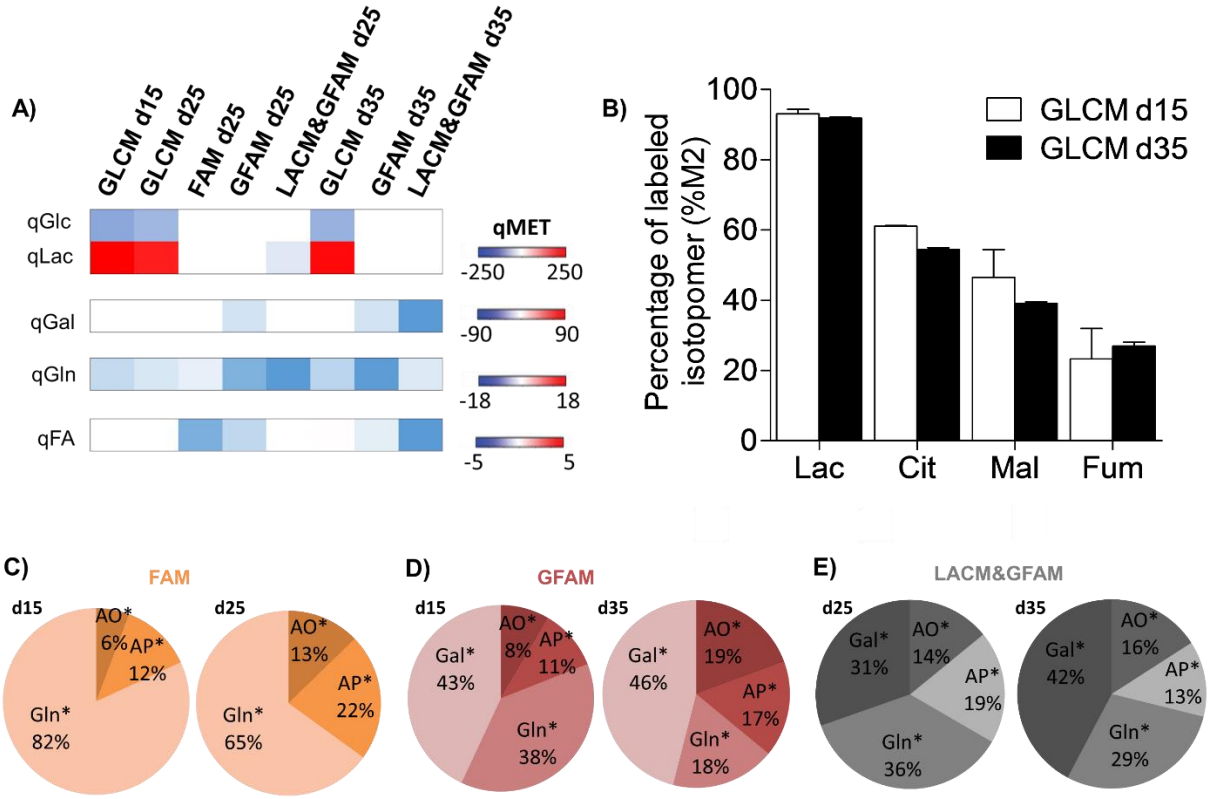

Figure 4.3 - Effect of culture medium composition on central carbon metabolism of hiPSC-CMs. (**A**) Heatmap image of metabolome data illustrating specific consumption (blue) and production (red) rates of metabolites (qMET; nmol/h/10^6cell). (**B**) Percentage of labelled M2 isotopomers from [1,2-^{13}C]Glc in lactate and TCA intermediates (citrate, fumarate, malate. (**C-E**) Pie charts reflecting the contribution of the main substrates present in each culture medium, for TCA cycle intermediates pools, at different timepoints. The percentages were determined based on the incorporation of each labelled substrate in citrate, fumarate and malate after 48h of incubation.

For hiPSC-CMs cultured in LACM&GFAM, the incorporation of fatty acids in TCA intermediates was similar at both d25 and d35 (approximately 30%) (Fig. 4.3 E). Since LACM&GFAM resembles substrate availability during heart development[35], these data could reflect what happens *in vivo*, as initial reliance in lactate oxidation may precondition hiPSC-CMs, allowing for a better adaptation to fatty acid metabolization upon initial exposure to this substrate. Like in GFAM, in LACM&GFAM condition, there is also a decrease in glutamine contribution concomitant with increased incorporation of [U-^{13}C]Gal, although to a lower degree, highlighting the increased role of fatty acids and galactose as fuel of TCA cycle in detriment of glutamine.

In order to comprehensively characterize fluxome changes of hiPSC-CMs cultured in distinct media, uptake and production rates along with ^{13}C incorporation data from parallel labelling experiments were integrated in a metabolic network model using nonstationary MFA[54]. At first glance, there is a remarkable difference between flux maps from GLCM and GFAM conditions at d35. In GLCM, hiPSC-CMs showed a highly glycolytic metabolism while in GFAM there is a higher reliance in TCA cycle along with a pronounced distribution of fluxes in other pathways like glycolysis and β-oxidation (Fig. 4.4 A and B). Importantly, hiPSC-CMs cultured in LACM&GFAM and GFAM had similar fluxomes at d35 (data not shown). Combination of fluxome and metabolome analyses reported herein with the transcriptomic data obtained from parallel experiments developed in the lab (Fig. S1), revealed that changes in metabolism were accompanied by alterations in metabolic gene expression.

In GFAM glycolytic fluxes decreased around 9-fold and fluxes of TCA cycle increased over 6-fold comparatively to GLCM. The glycolytic profile of GLCM is supported by up-regulation in the gene expression of key enzymes like SLC2A1, HK1/2 and ENO3 (Fig. S1), moreover virtually all of the cytosolic pyruvate is diverted to lactate secretion (491.4 in GLCM vs 0.0 nmol/(10^6 cells × h) in GFAM). In contrast, in GFAM, pyruvate is channeled to the mitochondria where it enters TCA cycle by conversion to Acetyl-CoA (67.2 in GFAM vs 5.6 nmol/(10^6 cells × h) in GLCM), also in this condition most of the enzymes involved in the TCA cycle are up-regulated (Fig. S1). Culture of different cell types, like muscle and cancer cells, in medium containing galactose has proved to enhance oxidative metabolism[53,69]. Despite relying in the same family of GLUT transporters, the uptake rate of galactose is markedly lower than that of glucose, due to low affinity of the transporters to galactose[70]. This results in a steep decrease in glycolytic flux, and consequent reduction in ATP production from anaerobic glycolysis, therefore cells increase their reliance on oxidative phosphorylation to maintain ATP levels[69].

Another important feature of GFAM metabolism, that is negligible in GLCM, is the increased oxidation of fatty acids (10.3 in GFAM vs 0.0 nmol/(10^6 cells × h) in GLCM) concomitant with a higher expression of enzymes involved in β-oxidation (Fig. S1), thus revealing an adaptation, also at the gene expression level, to more efficiently consume fatty acids.

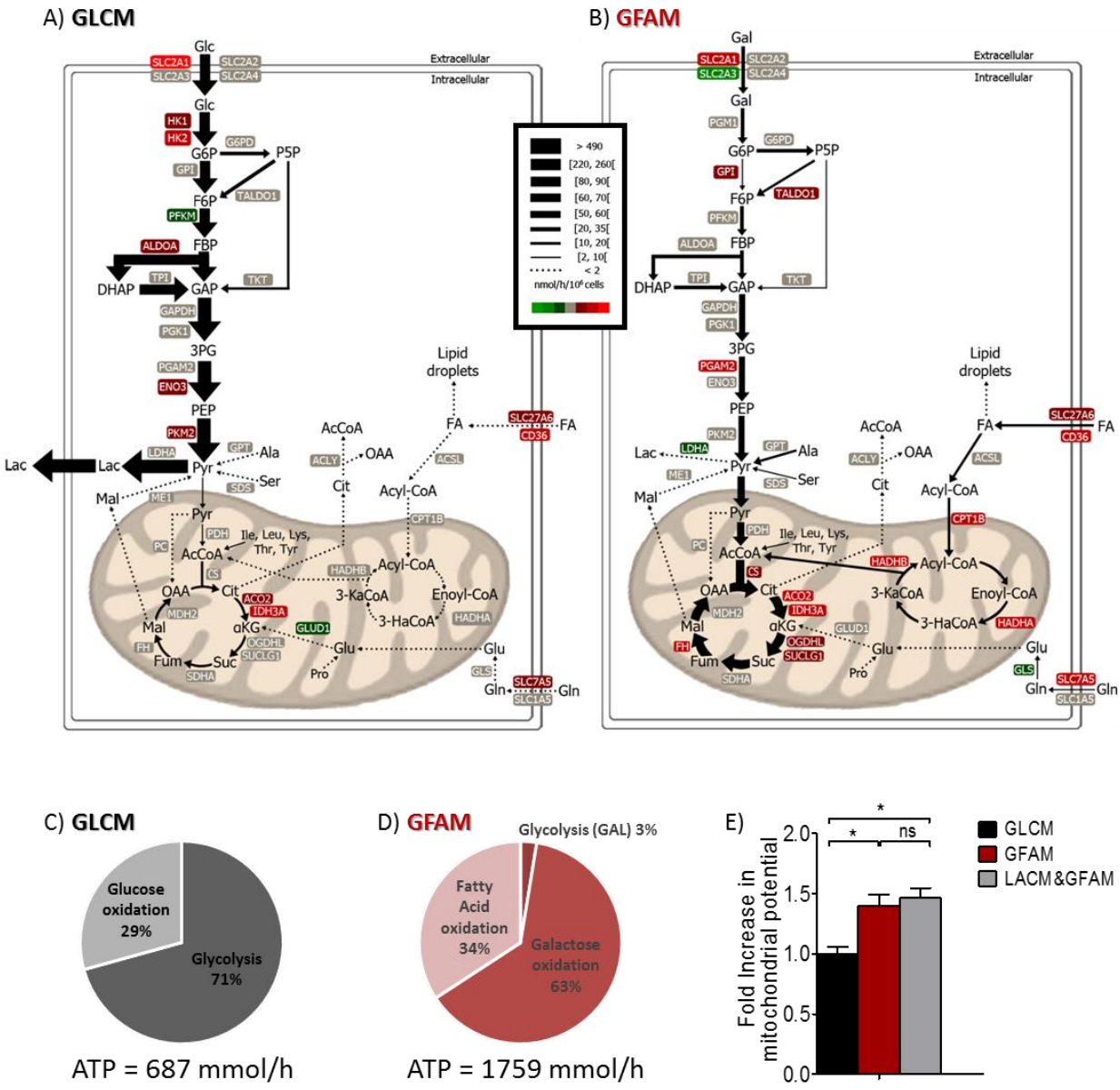

Figure 4.4 - Effect of culture media composition on the fluxome of hiPSC-CMs after maturation. Metabolic flux maps highlighting central carbon metabolism at d35 of hiPSC-CMs cultured in GLCM (**A**) and GFAM (**B**). Flux maps were determined using nonstationary ^{13}C-MFA analysis. Arrow thickness reflects flux values in units of nmol/h/10^{6}cell (see Table S1 for exact flux values). Up-regulated and down-regulated genes encoding metabolic enzymes are demarked in red and green, respectively. Genes were considered enriched based on a fold difference in expression (FC) ≥1.3 when compared with d15 (see Figure S1 for heatmap of FC from all culture conditions). Estimation of total ATP production and contribution of each metabolic pathway in GLCM (**C**) and GFAM (**D**). (**E**) Fold increase in mitochondrial membrane potential assessed at d35 by the increase in fluorescence intensity of the mitochondria specific dye, Mitoview. Fluorescence values were normalized for the values obtained in cells cultivated in GLCM. Data represented as mean±SD. *p<0.05; ns, not significant.

Even though flux through the Pentose Phosphate Pathway (PPP) is similar in GLCM and GFAM, it seems to have a greater relevance in the latter since approximately 70% of the glycolytic flux is diverted to PPP, contrasting with 13% in GLCM (Fig. 4.4 A and B). PPP is one of the main antioxidant cellular defense systems in cells and the higher estimated fluxes in GFAM may reflect an adaptation to prevent detrimental effects of increased production of free radicals promoted by the metabolic transition to aerobic respiration and oxidative phosphorilation[71]. Nonetheless, up-regulation of GPI and TALDO1 (Fig. S1) suggests that galactose was consumed through the glycolytic pathway (Fig. 4A and B).

The remodeling in metabolic profile is also evident in terms of estimated ATP production, which was determined by taking into account flux values estimated in nonstationary ^{13}C-MFA. In GLCM, 71% of total ATP produced derived from glycolysis, while in GFAM glycolysis corresponds to only 3% with the remaining 97% resulting from oxidative metabolism (Fig. 4.4 C and D). This improved reliance on oxidative metabolism increased 2.6-fold the total of ATP production in GFAM (1759 in GFAM vs 687 mmol/h in GLCM). Therefore this improvement may reflect a metabolic adaptation to comply with the increased energetic demand placed by hiPSC-CMs contractile function, as both cross-bridge and Ca^{2+} cycling are ATP-dependent processes[48].

To evaluate if the switch to an oxidative metabolism had any effect in mitochondria, cells were incubated with Mitoview, a fluorescent probe that acts as a reporter of mitochondrial membrane potential, which is crucial for maintaining ATP production[72]. Quantification of fluorescence intensity revealed a significant increase in membrane potential in both GFAM and LACM&GFAM comparatively to GLCM (Fig. 4.4 E), which indicates that in these conditions hiPSC-CMs displayed improved mitochondrial functionality. So, altogether this data indicates that hiPSC-CMs switch to an adult-like oxidative metabolism when cultured in GFAM and LACM&GFAM.

4.3. Supplementation of fatty acid medium with galactose prevents lipotoxicity

When cultured in FAM, hiPSC-CMs exhibited a significant decrease in viability at d25, reaching about only 10% of viable cells at d35 (Fig. 4.5 A), which compromised the analysis of cells at this time point. In fact, it has been reported in the literature that increased accumulation of fatty acids is associated with cardiac lipotoxicity[73]. As the increased uptake rate outpaces β-oxidation, there is an increased availability of fatty acids for the production of

cardiotoxic lipid metabolites that can directly or through activation of downstream pathways lead to cellular damage and toxicity[73].

To evaluate if decreased viability in FAM was a result of lipotoxicity, lipid accumulation was quantified through the use of a commercial kit that relies on Nile Red, a fluorescent dye specific for lipid droplets[74]. When compared with cells cultured in other media, hiPSC-CMs in FAM had a significant 4-fold increase in lipid droplet content (Fig. 4.5 B). Furthermore, flux map analysis confirms that most of fatty acid uptake (74%) is diverted for accumulation in lipid droplets, instead of b-oxidation (Fig. 4.5 C) even though gene expression of enzymes involved in this pathway is up-regulated (Fig. S1). Moreover central carbon metabolism is greatly altered, herein, TCA cycle is mainly fueled by amino acid carbon sources, mostly glutamate that replenishes α-ketoglutarate, since most citrate produced in TCA is transported to the cytosol. Also, pyruvate acquires an anaplerotic role to sustain TCA cycle activity by primarily producing oxaloacetate, as malate is shuttled to the cytosol where it is decarboxylated to pyruvate. Additionally, flux values estimated for glycolysis are supported by down-regulation of several enzymes involved in this pathway (Fig. S1). Even though fatty acids are the main substrate of the adult heart[35,52], culture of hiPSC-CMs in FAM seems to lead to a metabolic deregulation, which coupled with the lipotoxic effects of fatty acid accumulation could justify the decrease in cell viability.

Considering that galactose was proved to increase fatty acid oxidation and formation of neutral lipids in skeletal muscle cells[75], the absence of a marked accumulation of fatty acids or low viability in hiPSC-CMs cultured in GFAM suggests that galactose supplementation was enough to prevent lipotoxicity by improving oxidative capacity of hiPSC-CMs. Hence, improved oxidative capacity decreased fatty acid availability for non-oxidative pathways and consequent production of lipotoxic metabolites.

In future studies it would be interesting to investigate whether lipotoxicity in FAM arises from the medium composition itself or an inadequate adaptation of cells to an oxidative metabolism. This hypothesis could be tested by determining if pre-treatment of hiPSC-CMs with GFAM during for example 10 days, before switching to FAM, could prevent lipotoxicity.

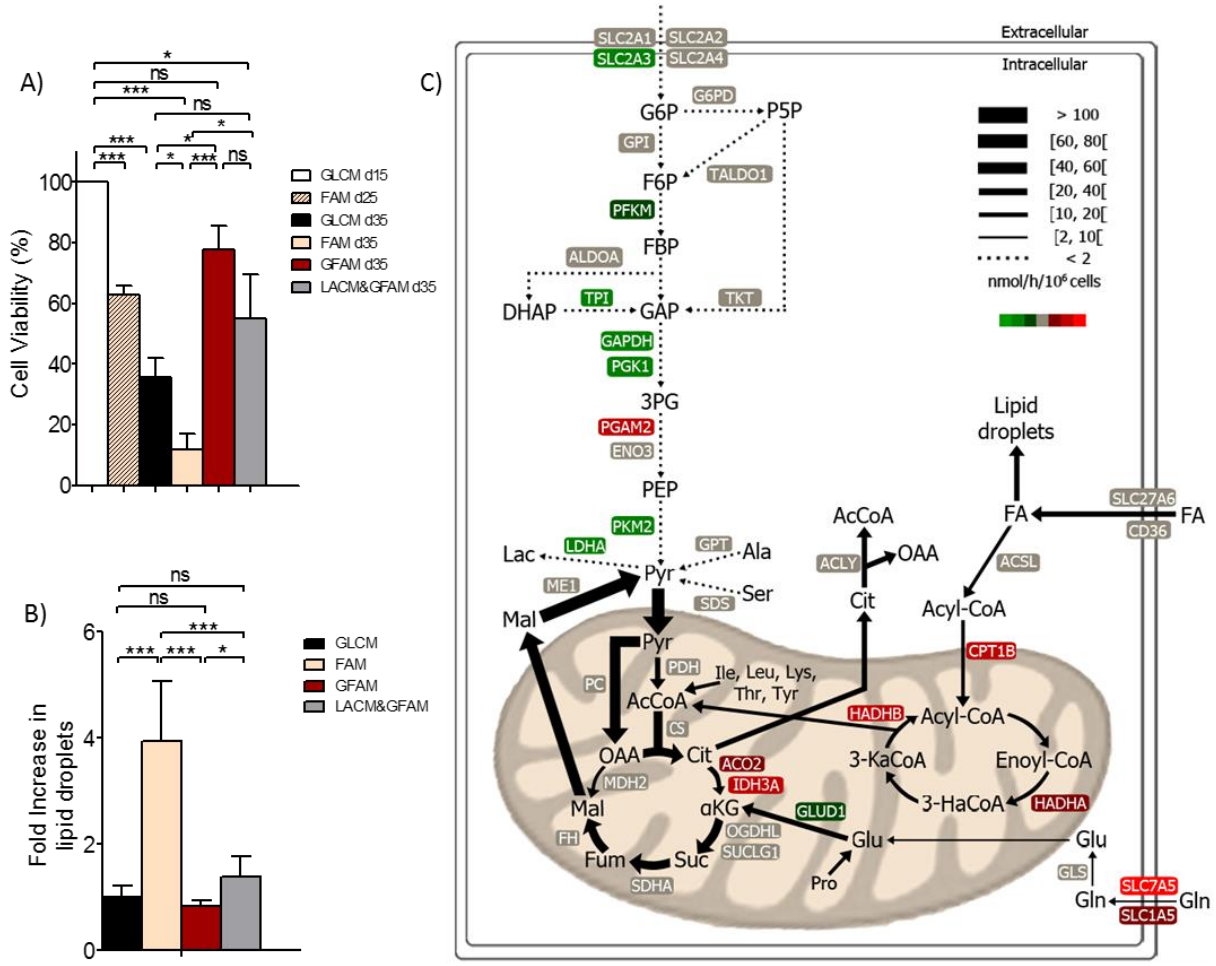

Figure 4.5 - Fatty acid rich medium induces lipotoxicity in hiPSC-CMs. (**A**) Percentage of cell viability in all culture conditions tested assessed using the Trypan Blue Exclusion Method. Cell viability is normalized to d15. (**B**) Analysis of lipid droplet content at d30 using a lipid droplet-specific fluorescent dye, Nile Red. Fluorescence values were normalized for the values obtained in cells cultivated in GLCM. (**C**) Metabolic flux map highlighting central carbon metabolism of hiPSC-CMs cultivated in FAM at d25. The flux map was determined using nonstationary ^{13}C-MFA analysis. Arrow thickness reflects flux values in units of nmol/h/10^{6}cell (see Table S1 for exact flux values). Up-regulated and down-regulated genes encoding metabolic enzymes are demarked in red and green, respectively. Genes were considered enriched based on a fold difference in expression (FC) ≥1.3 when compared with d15 (see Figure S1 for heatmap of FC from all culture conditions). Data represented as mean±SD. *p<0.05; ***p<0.001; ns, not significant.

4.4. GFAM improves morphology and structure of hiPSC-CMs

Analysis of hiPSC-CMs morphology throughout culture time revealed that in contrast with GLCM, cells cultured in the others glucose depleted media exhibit lower surface area and circularity, and a higher length-to-width ratio (Fig. 4.6 A-C). Thus hiPSC-CMs cultured in these conditions, showed morphological features resembling adult cardiomyocytes, which have an elongated rod-like shape with length-to-width ratios in the range of 7-9.5[42].

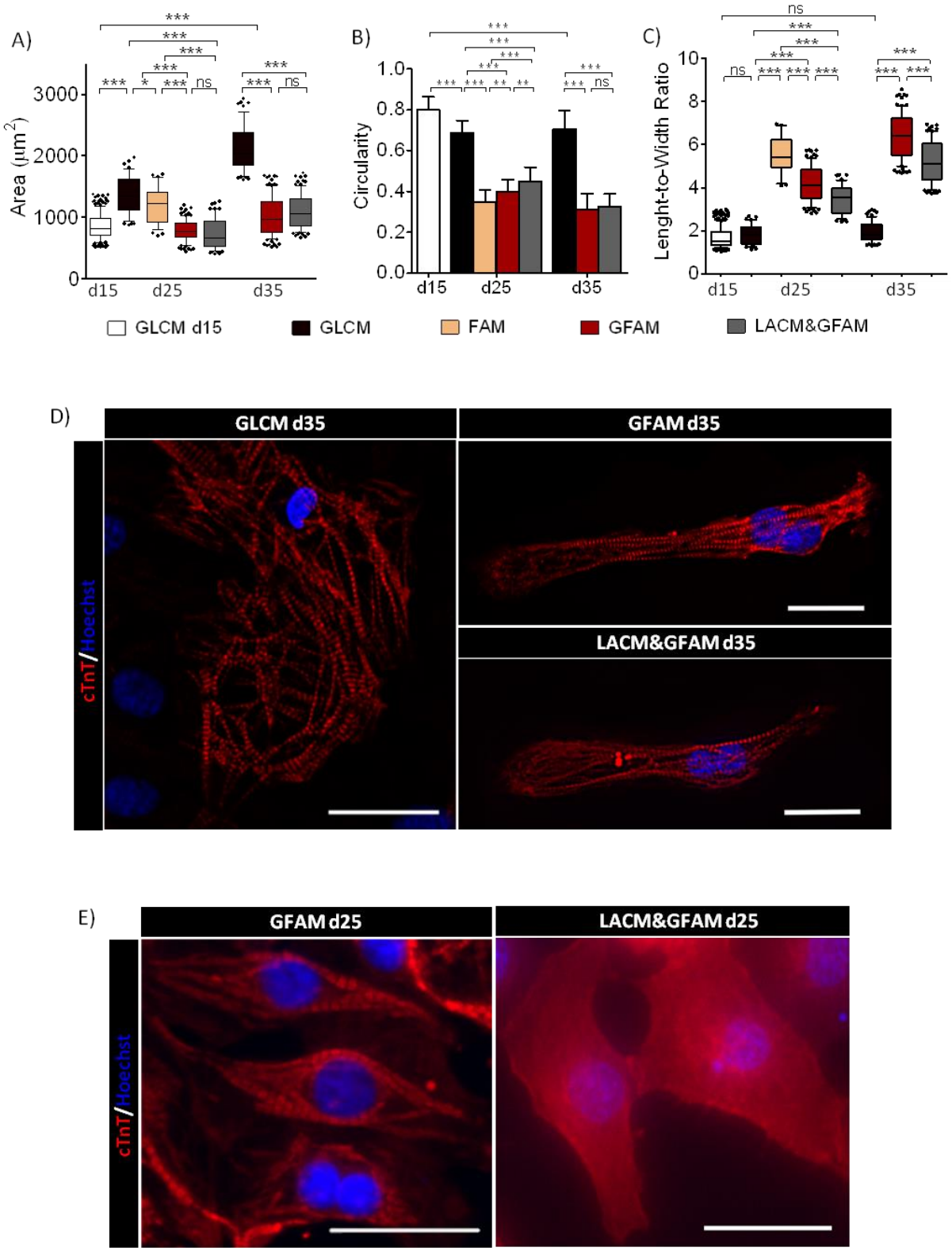

Figure 4.6 – Morphology and structural features of hiPSC-CMs after culture in different media. (**A-C**) Cell structure characterization in terms of cell area (**A**), circularity index (**B**) and length-to-width ratio (**C**). n>70 cells per condition. Representative images of hPSC-CMs immunostained for cardiac troponin-T (cTnT, red), at d35 (**D**) and d25 (**E**) of culture in different media. Nuclei (blue) were stained with Hoechst 33342. Scale bars = 30 µm. Data represented as mean±SD. *p<0.05; **p<0.01; ***p<0.001; ns, not significant.

Immunofluorescence microscopy analysis highlights that besides the large area and round shape observed, cells in GLCM display disorganized sarcomeres (Fig. 4.6 D-left panel), all of which reminiscent of pathogenic hypertrophy[44]. Therefore, maintenance of hiPSC-CMs in glucose rich medium appears to have detrimental effects on maturation not only because cells remain highly glycolytic (Fig 4.4 A), resembling human fetal cardiomyocytes[32], but also due to the development of pathogenic hypertrophy.

In contrast, hiPSC-CMs cultured in GFAM and LACM&GFAM exhibited highly organized sarcomeres, spanning in parallel across all cell (Fig. 4.6 D-right panels). However, in LACM&GFAM the cross-striated pattern of cTnT is less defined. In fact, at d25, cTnT staining is very diffuse in LACM&GFAM (Fig. 4.6 E-right panel), contrasting with GFAM where a cross-striated pattern of sarcomeres is already evident (Fig. 4.6 E-left panel). This data suggests that, culture of hiPSC-CMs in LACM&GFAM until d25 did not suffice to induce the same degree of structural maturation as culture in GFAM did. However, at d35 cells cultured in LACM&GFAM displayed considerable improvements in sarcomere organization (Fig. 4.6 D-bottom right panel). Since hiPSC-CMs maintained in the LACM&GFAM feeding strategy are cultured in GFAM from d25 to d35, these results highlight the importance of GFAM medium composition in hiPSC-CMs structural maturation. Therefore, LACM&GFAM could be an appropriate maturation strategy if the purity of the initial hiPSC-CM culture is low, as the first 10 days in lactate allow for the metabolic selection of hiPSC-CM, as reported previously by others[32]. Since in this study the starting population was highly pure, the rationale of using lactate was to mimic substrate availability during heart development[35] and ascertain if it would increase maturation. However, this strategy proved less efficient than maintaining hiPSC-CMs in GFAM during 20 days.

When comparing d35 to d25 in GFAM, hiPSC-CMs features present significant improvements in metabolic and structural maturation, raising the question if increased culture time in GFAM could bring further improvements in hiPSC-CMs maturation, however this notion still requires additional investigation. Nevertheless, culture of hiPSC-CMs in GFAM proved to be a time efficient strategy since 20 days of culture were enough to achieve substantial improvements in hiPSC-CM structural and metabolic maturation.

The work presented in this thesis showed that a simple change in carbon source induced a shift to an oxidative metabolism that was accompanied by increased structural maturation of hiPSC-CMs, evidencing the link between regulation of metabolism and hiPSC-CMs maturation *in vitro*. Furthermore, it is important to mention that in parallel to this work, functional analyses of hiPSC-CMs were carried out in collaboration with Dr. Ibrahim

Domian, to evaluate calcium, contractility and action potential kinetics and confirm functional maturation of hiPSC-CMs.

The maturation protocol established in this study holds technical and economic advantages over the existing protocols due to its simplicity (a simple medium-exchange procedure) and ease of application (does not require specific equipment or addition of expensive factors/chemicals). Moreover, it can be easily combined with other approaches, like mechanical[41] and electrical stimulation[42], to further improve hiPSC-CMs maturation *in vitro* by mimicking the wide range of factors that come into play during heart development *in vivo*. Additionally, it is noteworthy that 10 days of culture in GFAM was sufficient to promote hiPSC-CM metabolic and structural maturation comparable to what has been described in the literature after 80-100 days of culture[76]. Therefore GFAM treatment constitutes a great advance for the maturation of hiPSC-CMs in a time efficient manner. This will strengthen the potential of hiPSC-CMs application in cell therapy, drug discovery, toxicity testing and cardiac disease modeling.

5. Conclusion

In this study a new approach for hiPSC-CMs maturation was developed by changing the carbon source available in cell culture medium.

hPSC-CMs remained highly glycolytic regardless of the evident development in metabolic machinery during differentiation. However, upon culture in distinct glucose depleted media, hiPSC-CMs exhibited remarkable metabolic plasticity switching to an oxidative metabolism. Therefore, these results suggest that when the main substrate available in the media is glucose, the preferred consumption of this substrate restricts hiPSC-CMs metabolism to a glycolytic profile.

From the distinct selection of media tested, culture in GFAM was the most efficient strategy in improving hiPSC-CMs maturation *in vitro*, with cells displaying a more energetically efficient oxidative metabolism, elongated morphologies and organized sarcomeric structures. Moreover, supplementation of fatty acid medium with galactose increased hiPSC-CMs oxidative capacity, improving fatty acid oxidation and preventing lipotoxic effects of excessive fatty acid accumulation. In the standard glucose supplemented medium, hiPSC-CMs maintained a fetal-like metabolic profile and showed features that resemble pathogenic hypertrophy. These results highlight the regulatory role of metabolism in a wide range of vital cellular functions.

To date, no other study has established a quantitative metabolic network model, using nonstationary ^{13}C-MFA, of hiPSC-CMs cultured in distinct carbon sources, nor the extent to which this change modulates metabolic and structural maturation of hiPSC-CMs, as assessed herein. Furthermore, 10 days of culture in GFAM was sufficient to promote hiPSC-CM metabolic and structural maturation comparable to what has been described in the literature after long term culture. Thus, the protocol developed herein represents a relevant step forward in time efficient maturation of hiPSC-CMs, bridging closer the gap between hiPSC-CMs and cell therapy or pre-clinical applications.

Future investigations relying on the combination of this maturation strategy with a 3D cell culture approach using environmentally controlled bioreactors will be pursued as a promising strategy towards the scalable production of more mature hiPSC-CMs *in vitro*.

6. References

1. WHO. Global status report on noncommunicable diseases 2014. *World Health* 176 (2014).
2. Chien, K. R. & Olson, E. N. Converging pathways and principles in heart development and disease. in *Cell* **110,** 153–162 (2002).
3. Saraste, A. *et al.* Cardiomyocyte apoptosis and progression of heart failure to transplantation. *Eur. J. Clin. Invest.* **29,** 380–386 (1999).
4. Beltrami, A. P. *et al.* Adult cardiac stem cells are multipotent and support myocardial regeneration. *Cell* **114,** 763–776 (2003).
5. Bergmann, O. *et al.* Evidence for cardiomyocyte renewal in humans. *Science* **324,** 98–102 (2009).
6. Deb, A. & Ubil, E. Cardiac fibroblast in development and wound healing. *Journal of Molecular and Cellular Cardiology* **70,** 47–55 (2014).
7. Evans, M. J. & Kaufman, M. H. Establishment in culture of pluripotential cells from mouse embryos. *Nature* **292,** 154–156 (1981).
8. Thomson, J. A. *et al.* Embryonic stem cell lines derived from human blastocysts. *Science* **282,** 1145–1147 (1998).
9. Chong, J. J. H. *et al.* Human embryonic-stem-cell-derived cardiomyocytes regenerate non-human primate hearts. *Nature* **510,** 273–7 (2014).
10. Miyahara, Y. *et al.* Monolayered mesenchymal stem cells repair scarred myocardium after myocardial infarction. *Nat. Med.* **12,** 459–465 (2006).
11. Orlic, D. *et al.* Bone marrow cells regenerate infarcted myocardium. *Nature* **410,** 701–705 (2001).
12. Menasche, P. *et al.* Human embryonic stem cell-derived cardiac progenitors for severe heart failure treatment: First clinical case report. *Eur. Heart J.* **36,** 2011–2017 (2015).
13. Burgess, R. *Stem Cells Handbook*. *Humana Press*, Springer New York, (2013).
14. Takahashi, K. & Yamanaka, S. Induction of Pluripotent Stem Cells from Mouse Embryonic and Adult Fibroblast Cultures by Defined Factors. *Cell* **126,** 663–676 (2006).
15. Takahashi, K. *et al.* Induction of Pluripotent Stem Cells from Adult Human Fibroblasts by Defined Factors. *Cell* **131,** 861–872 (2007).
16. Ueno, S. *et al.* Biphasic role for Wnt/beta-catenin signaling in cardiac specification in zebrafish and embryonic stem cells. *Proc. Natl. Acad. Sci. U. S. A.* **104,** 9685–9690 (2007).
17. Drawnel, F. M. *et al.* Disease modeling and phenotypic drug screening for diabetic cardiomyopathy using human induced pluripotent stem cells. *Cell Rep.* **9,** 810–820 (2014).
18. Laflamme, M. a *et al.* Cardiomyocytes derived from human embryonic stem cells in pro-survival factors enhance function of infarcted rat hearts. *Nat. Biotechnol.* **25,** 1015–1024 (2007).
19. Kehat, I. *et al.* Human embryonic stem cells can differentiate into myocytes with structural and functional properties of cardiomyocytes. *J. Clin. Invest.* **108,** 407–14 (2001).
20. Mummery, C. *et al.* Differentiation of human embryonic stem cells to cardiomyocytes: role of coculture with visceral endoderm-like cells. *Circulation* **107,** 2733–40 (2003).
21. Lian, X. *et al.* Robust cardiomyocyte differentiation from human pluripotent stem cells via temporal modulation of canonical Wnt signaling. *Proc. Natl. Acad. Sci. U. S. A.* **109,** E1848-57 (2012).
22. Kattman, S. J. *et al.* Stage-specific optimization of activin/nodal and BMP signaling promotes cardiac differentiation of mouse and human pluripotent stem cell lines. *Cell Stem Cell* **8,** 228–240 (2011).
23. Kadari, A. *et al.* Robust generation of cardiomyocytes from human iPS cells requires precise modulation of BMP and WNT signaling. *Stem Cell Rev. Reports* **11,** 560–569 (2015).
24. Kamps, J. A. & Krenning, G. Micromanaging cardiac regeneration: Targeted delivery of microRNAs for cardiac repair and regeneration. *World J. Cardiol.* **8,** 163–79 (2016).
25. Burridge, P. W. *et al.* Chemically defined generation of human cardiomyocytes. *Nat. Methods* **11,** 855–60 (2014).
26. Paige, S. L. *et al.* Endogenous Wnt/beta-catenin signaling is required for cardiac differentiation

in human embryonic stem cells. *PLoS One* **5,** e11134 (2010).
27. Fujikawa, T. *et al.* Teratoma formation leads to failure of treatment for type I diabetes using embryonic stem cell-derived insulin-producing cells. *Am J Pathol* **166,** 1781–1791 (2005).
28. Xu, C. Characterization and Enrichment of Cardiomyocytes Derived From Human Embryonic Stem Cells. *Circ. Res.* **91,** 501–508 (2002).
29. Skelton, R. J. P. *et al.* SIRPA, VCAM1 and CD34 identify discrete lineages during early human cardiovascular development. *Stem Cell Res.* **13,** 172–179 (2014).
30. Hattori, F. *et al.* Nongenetic method for purifying stem cell–derived cardiomyocytes. *Nat. Methods* **7,** 61–66 (2010).
31. Wile, B. M., Ban, K., Yoon, Y.-S. & Bao, G. Molecular beacon-enabled purification of living cells by targeting cell type-specific mRNAs. *Nat. Protoc.* **9,** 2411–24 (2014).
32. Tohyama, S. *et al.* Distinct metabolic flow enables large-scale purification of mouse and human pluripotent stem cell-derived cardiomyocytes. *Cell Stem Cell* **12,** 127–137 (2013).
33. Snir, M. *et al.* Assessment of the ultrastructural and proliferative properties of human embryonic stem cell-derived cardiomyocytes. *Am J Physiol Hear. Circ Physiol* **285,** 55-63 (2003).
34. Synnergren, J., Améen, C., Jansson, A. & Sartipy, P. Global transcriptional profiling reveals similarities and differences between human stem cell-derived cardiomyocyte clusters and heart tissue. *Physiol. Genomics* **44,** 245–58 (2012).
35. Lopaschuk, G. D. & Jaswal, J. S. Energy metabolic phenotype of the cardiomyocyte during development, differentiation, and postnatal maturation. *J. Cardiovasc. Pharmacol.* **56,** 130–40 (2010).
36. Brito-Martins, M., Harding, S. E. & Ali, N. N. Beta(1)- and Beta(2)-Adrenoceptor Responses in Cardiomyocytes Derived from Human Embryonic Stem Cells: Comparison with Failing and Non-Failing Adult Human Heart . *Br. J. Pharmacol.* **153,** 751–759 (2008).
37. White, M. C., Pang, L. & Yang, X. MicroRNA-mediated maturation of human pluripotent stem cell-derived cardiomyocytes: Towards a better model for cardiotoxicity? *Food Chem. Toxicol.* (2016).
38. Kuppusamy, K. T. *et al.* Let-7 family of microRNA is required for maturation and adult-like metabolism in stem cell-derived cardiomyocytes. *Proc. Natl. Acad. Sci.* 201424042 (2015).
39. Yang, X. *et al.* Tri-iodo-l-thyronine promotes the maturation of human cardiomyocytes-derived from induced pluripotent stem cells. *J. Mol. Cell. Cardiol.* **72,** 296–304 (2014).
40. Mihic, A. *et al.* The effect of cyclic stretch on maturation and 3D tissue formation of human embryonic stem cell-derived cardiomyocytes. *Biomaterials* **35,** 2798–2808 (2014).
41. Heidi Au, H. T., Cui, B., Chu, Z. E., Veres, T. & Radisic, M. Cell culture chips for simultaneous application of topographical and electrical cues enhance phenotype of cardiomyocytes. *Lab Chip* **9,** 564–575 (2009).
42. Gerdes, A. M. *et al.* Structural remodeling of cardiac myocytes in patients with ischemic cardiomyopathy. *Circulation* **86,** 426–430 (1992).
43. Chung, C. Y., Bien, H. & Entcheva, E. The role of cardiac tissue alignment in modulating electrical function. *J. Cardiovasc. Electrophysiol.* **18,** 1323–1329 (2007).
44. Dorn, G. W., Robbins, J. & Sugden, P. H. Phenotyping hypertrophy: Eschew obfuscation. *Circ. Res.* **92,** 1171–1175 (2003).
45. Engelhardt, S., Hein, L., Wiesmann, F. & Lohse, M. J. Progressive hypertrophy and heart failure in beta1-adrenergic receptor transgenic mice. *Proc. Natl. Acad. Sci. U. S. A.* **96,** 7059–64 (1999).
46. Huxley, H. E. The crossbridge mechanism of muscular contraction and its implications. *J. Exp. Biol.* **115,** 17–30 (1985).
47. Feric, N. T. & Radisic, M. Maturing human pluripotent stem cell-derived cardiomyocytes in human engineered cardiac tissues. *Advanced Drug Delivery Reviews* **96,** 110–134 (2016).
48. Altamirano, J. & Bers, D. M. Voltage dependence of cardiac excitation-contraction coupling: Unitary Ca2+ current amplitude and open channel probability. *Circ. Res.* **101,** 590–597 (2007).
49. Yang, Z., Yamazaki, M., Shen, Q. W. & Swartz, D. R. Differences between cardiac and skeletal troponin interaction with the thin filament probed by troponin exchange in skeletal myofibrils. *Biophys. J.* **97,** 183–194 (2009).

50. Martini, F., Nath, J. & Bartholomew, E. *Fundamentals of Anatomy and Physiology*. *Benjamin Cummings* **9th,** (2011).
51. Schönfeld, P., Schild, L. & Bohnensack, R. Expression of the ADP/ATP carrier and expansion of the mitochondrial (ATP + ADP) pool contribute to postnatal maturation of the rat heart. *Eur. J. Biochem.* **241,** 895–900 (1996).
52. Kolwicz, S. C., Purohit, S. & Tian, R. Cardiac metabolism and its interactions with contraction, growth, and survival of cardiomyocytes. *Circulation Research* **113,** 603–616 (2013).
53. Rana, P., Anson, B., Engle, S. & Will, Y. Characterization of Human Induced Pluripotent Stem Cell Derived Cardiomyocytes: Bioenergetics and Utilization in Safety Screening. *Toxicol. Sci.* **130,** 117–31 (2012).
54. Woo Suk, A. & Antoniewicz, M. R. Parallel labeling experiments with [1,2-13C]glucose and [U-13C]glutamine provide new insights into CHO cell metabolism. *Metab. Eng.* **15,** 34–47 (2013).
55. Goudar, C. *et al.* Metabolic flux analysis of CHO cells in perfusion culture by metabolite balancing and 2D [13C, 1H] COSY NMR spectroscopy. *Metab. Eng.* **12,** 138–149 (2010).
56. Antoniewicz, M. R., Kelleher, J. K. & Stephanopoulos, G. Elementary metabolite units (EMU): A novel framework for modeling isotopic distributions. *Metab. Eng.* **9,** 68–86 (2007).
57. Carinhas, N. *et al.* Metabolic flux profiling of MDCK cells during growth and canine adenovirus vector production. *Sci. Rep.* **6,** 1–11 (2016).
58. Hofmann, U., Maier, K., Reuss, M. & Mauch, K. Identification of metabolic fluxes in hepatic cells from transient 13C-labeling experiments: Part II. Flux estimation. *Biotechnol. Bioeng.* **100,** 355–370 (2008).
59. Elliott, D. A. *et al.* NKX2-5(eGFP/w) hESCs for isolation of human cardiac progenitors and cardiomyocytes. *Nat. Methods* **8,** 1037–40 (2011).
60. Correia, C. *et al.* Effective Hypothermic Storage of Human Pluripotent Stem Cell-Derived Cardiomyocytes Compatible With Global Distribution of Cells for Clinical Applications and Toxicology Testing. *Stem Cells Transl. Med.* **5,** 658–69 (2016).
61. Qiagen. Ingenuity. (2016). Available at: http://www.ingenuity.com/.
62. Carinhas, N. *et al.* Improving baculovirus production at high cell density through manipulation of energy metabolism. *Metab. Eng.* **12,** 39–52 (2010).
63. Young, J. D. INCA: A computational platform for isotopically non-stationary metabolic flux analysis. *Bioinformatics* **30,** 1333–1335 (2014).
64. Nelson, D. L. & Cox, M. M. *Lehninger Principles of Biochemistry 6th ed. Humana Press*, Springer New York (2013).
65. Salazar-Cantú, A. *et al.* Role of SERCA and the sarcoplasmic reticulum calcium content on calcium waves propagation in rat ventricular myocytes. *Arch. Biochem. Biophys.* **604,** 11–19 (2016).
66. Ebert, A. M. *et al.* Calcium extrusion is critical for cardiac morphogenesis and rhythm in embryonic zebrafish hearts. *Proc. Natl. Acad. Sci. U. S. A.* **102,** 17705–10 (2005).
67. Thompson, B. R., Houang, E. M., Sham, Y. Y. & Metzger, J. M. Molecular determinants of cardiac myocyte performance as conferred by isoform-specific tni residues. *Biophys. J.* **106,** 2105–2114 (2014).
68. Zhu, F.-Y. *et al.* SWATH-MS Quantitative Proteomic Investigation Reveals a Role of Jasmonic Acid during Lead Response in Arabidopsis. *J. Proteome Res.* (2016).
69. Aguer, C. *et al.* Galactose enhances oxidative metabolism and reveals mitochondrial dysfunction in human primary muscle cells. *PLoS One* **6,** (2011).
70. Zhao, F.-Q. & Keating, A. F. Functional properties and genomics of glucose transporters. *Curr. Genomics* **8,** 113–28 (2007).
71. Riganti, C., Gazzano, E., Polimeni, M., Aldieri, E. & Ghigo, D. The pentose phosphate pathway: An antioxidant defense and a crossroad in tumor cell fate. *Free Radic. Biol. Med.* **53,** 421–436 (2012).
72. Dimroth, P., Kaim, G. & Matthey, U. Crucial role of the membrane potential for ATP synthesis by F(1)F(o) ATP synthases. *J. Exp. Biol.* **203,** 51–59 (2000).
73. Chiu, H. C. *et al.* Transgenic expression of fatty acid transport protein 1 in the heart causes lipotoxic cardiomyopathy. *Circ. Res.* **96,** 225–233 (2005).

74. Listenberger, L. L. & Brown, D. a. Fluorescent detection of lipid droplets and associated proteins. *Curr. Protoc. Cell Biol.* **24,** (2007).
75. Kase, E. T. *et al.* Remodeling of Oxidative Energy Metabolism by Galactose Improves Glucose Handling and Metabolic Switching in Human Skeletal Muscle Cells. *PLoS One* **8,** (2013).
76. Lundy, S. D., Zhu, W.-Z., Regnier, M. & Laflamme, M. A. Structural and functional maturation of cardiomyocytes derived from human pluripotent stem cells. *Stem Cells Dev.* **22,** 1991–2002 (2013).

7. Annexes

Table S1 - Metabolic network reactions and simulated fluxes determined by nonstationary ^{13}C-MFA. Flux values are shown in units of nmol/h/10^6cell. Negative flux values indicate that net direction is reverse to the direction indicated.

Reactions		Flux values		
		GLCM d35	GFAM d35	FAM d35
v1	G6P <-> F6P	220.45	9.01	0.00
v2	F6P -> FBP	242.93	22.68	0.00
v3	FBP <-> DHAP + GAP	242.93	22.68	0.00
v4	DHAP <-> GAP	242.93	22.68	0.00
v5	GAP <-> 3PG	497.10	52.20	0.00
v6	3PG <-> PEP	496.94	52.20	0.00
v7	PEP -> Pyr.c	496.94	52.20	0.00
v8	Pyr.c <-> Pyr.m	5.59	67.33	102.50
v9	G6P -> P5P + CO2	33.72	20.50	0.00
v10	P5P + P5P <-> GAP + S7P	11.24	6.83	0.00
v11	S7P + GAP <-> E4P + F6P	11.24	6.83	0.00
v12	E4P + P5P <-> GAP + F6P	11.24	6.83	0.00
v13	Pyr.c <-> Lac	491.38	0.00	0.00
v14	Pyr.c <-> Ala	-0.03	-11.02	0.00
v15	Pyr.m -> AcCoA.m + CO2	5.59	67.15	30.01
v16	OAA.m + AcCoA.m -> Cit.m	14.14	87.87	55.04
v17	Cit.m <-> AKG + CO2	14.09	87.44	21.93
v18	AKG -> SucCoA + CO2	14.70	87.03	42.92
v19	SucCoA <-> Suc	14.70	87.03	42.92
v20	Suc <-> Fum.m	14.70	87.27	45.30
v21	Fum.m <-> Mal.m	14.70	87.69	51.66
v22	Mal.m <-> OAA.m	14.14	87.69	-17.45
v23	Mal.c -> Pyr.c + CO2	0.00	0.43	102.22
v24	Pyr.m + CO2 -> OAA.m	0.00	0.18	72.49
v25	Gln <-> Glu	0.99	2.47	3.83
v26	AKG <-> Glu	-0.61	0.41	-20.99
v27	Asn <-> Asp	0.00	0.00	0.00
v28	3PG -> Ser	0.16	0.00	0.00
v29	Ser -> Pyr.c	0.00	3.68	0.28
v30	Ser <-> Gly + C1	-1.78	-1.02	-2.39
v31	Glu <-> Pro	0.00	0.98	-10.49
v32	Val + CO2 -> Suc + CO2 + CO2	0.00	0.13	0.00
v33	Ile + CO2 -> Suc + AcCoA.m + CO2	0.00	0.00	0.00
v34	Leu + CO2 -> AcCoA.m + AcCoA.m + AcCoA.m + CO2	2.25	1.54	0.00
v35	Thr -> AcCoA.m + Gly	0.00	0.34	3.93
v36	Phe -> Tyr	0.00	0.06	0.00

v37	Tyr -> Fum.m + AcCoA.m + AcCoA.m + CO2	0.00	0.42	6.36
v38	Met + Ser + CO2 -> Suc + Cys.snk + CO2 + C1	0.00	0.12	2.39
v39	Lys -> CO2 + CO2 + AcCoA.m + AcCoA.m	0.90	2.36	0.00
v40	His -> Glu + C1	1.78	0.90	0.00
v41	Arg -> Glu + Urea.snk	59.81	58.67	0.00
v42	Glu + CO2 -> Arg	63.96	61.80	0.00
v43	Glc.ext -> G6P	254.17	0.00	0.00
v44	Lac.ext <-> Lac	-491.38	0.00	0.00
v45	Ala.ext <-> Ala	0.03	11.02	0.00
v46	Gln.ext -> Gln	0.99	2.47	3.83
v47	Glu.ext <-> Glu	1.99	0.33	6.68
v48	Ser.ext <-> Ser	-1.93	2.78	0.28
v49	Gly.ext <-> Gly	1.78	0.67	-1.55
v50	Pro.ext <-> Pro	0.00	-0.98	10.49
v51	Val.ext -> Val	0.00	0.13	0.00
v52	Ile.ext -> Ile	0.00	0.00	0.00
v53	Leu.ext -> Leu	2.25	1.54	0.00
v54	Thr.ext -> Thr	0.00	0.34	3.93
v55	Phe.ext -> Phe	0.00	0.06	0.00
v56	Tyr.ext -> Tyr	0.00	0.35	6.36
v57	Met.ext -> Met	0.00	0.12	2.39
v58	Lys.ext -> Lys	0.90	2.36	0.00
v59	His.ext -> His	1.78	0.90	0.00
v60	Arg.ext <-> Arg	-4.15	-3.13	0.00
v61	Asp <-> OAA.c	-0.61	0.00	0.00
v62	Cit.c -> OAA.c + AcCoA.c	0.05	0.43	33.11
v63	CO2.ext <-> CO2	-5.94	-50.84	-130.96
v64	AcCoA.c -> FA.ext	0.05	0.43	33.11
v65	PA.ext -> PA.c	0.00	5.21	16.74
v66	PA.m -> AcCoA.m + AcCoA.m + AcCoA.m + AcCoA.m + AcCoA.m + AcCoA.m + AcCoA.m + AcCoA.m	0.00	4.92	5.18
v67	OA.ext -> OA.c	0.00	5.51	15.60
v68	OA.m -> AcCoA.m + AcCoA.m + AcCoA.m + AcCoA.m + AcCoA.m + AcCoA.m + AcCoA.m + AcCoA.m + AcCoA.m	0.00	5.29	3.20
v69	Gal.ext -> G6P	0.00	29.51	0.00
v70	Cit.c -> Cit.snk	0.00	0.00	0.00
v71	Mal.m <-> Mal.c	0.56	0.00	69.11
v72	0*Mal.c -> Mal.s	3.93	0.00	0.00
v73	0*Mal.m -> Mal.s	96.07	100.00	100.00
v74	Mal.s -> Sink	100.00	100.00	100.00
v75	0*Fum.c -> Fum.s	14.02	30.52	0.00

v76	0*Fum.m -> Fum.s	85.98	69.48	100.00
v77	Fum.s -> Sink	100.00	100	100.00
v78	Mal.c <-> Fum.c	0.00	0.00	0.00
v79	OAA.c <-> Mal.c	-0.56	0.43	33.11
v80	Asp.ext <-> Asp	-0.61	0.00	0.00
v81	0*Cit.c -> Cit.s	0.00	96.40	0.00
v82	0*Cit.m -> Cit.s	100.00	3.60	100.00
v83	Cit.s -> Sink	100.00	100.00	100.00
v84	Cit.c <-> Cit.m	-0.05	-0.43	-33.11
v85	PA.c -> PA.m	0.00	0.62	0.65
v86	PA.c -> PA.snk	0.00	0.59	0.36
v87	OA.c -> OA.m	0.00	0.04	1.45
v88	OA.c -> OA.snk	0.00	0.02	1.38

Abbreviations: c. cytosolic; m. mitochondrial; s. sink.

Fumarate and succinate were considered as symmetric molecules during flux estimation. Compartmentalization of Pyr, Fum, Mal, Cit, AcCoA, OAA, AO and AP pools were taken into account in the model. Sink pools were considered for metabolites that could not be balanced.

Balanced metabolite pools: G6P, F6P, FBP, DHAP, GAP, 3PG, PEP, Pyr.c, Pyr.m, P5P, CO2, S7P, E4P, Lac, Ala, AO.c, AO.m, AP.c, AP.m, AcCoA.c, AcCoA.m, OAA.c,OAA.m, Pyr.c, Pyr.m, Cit.c, Cit.m, AKG, SucCoA, Suc, Fum.c, Fum.m, Mal.c,Mal.m, Gln, Glu, Asn, Asp, Ser, Gly, C1, Pro, Val, Ile, Leu, Thr, Phe, Tyr, Met, Lys, His, Arg.

Unbalanced metabolite pools: AO.ext, AP.ext, Ao.snk, Ap.snk, Cit.snk, FA.ext, CO2.ext, Glc.ext, Gal.ext Lac.ext, Ala.ext, Gln.ext, Glu.ext, Asp.ext, Asn.ext, Ser.ext, Gly.ext, Pro.ext, Val.ext, Ile.ext, Leu.ext, Thr. ext, Phe.ext, Tyr.ext, Met.ext, Lys.ext, His.ext, Arg.ext, Cys.snk, Urea.snk.

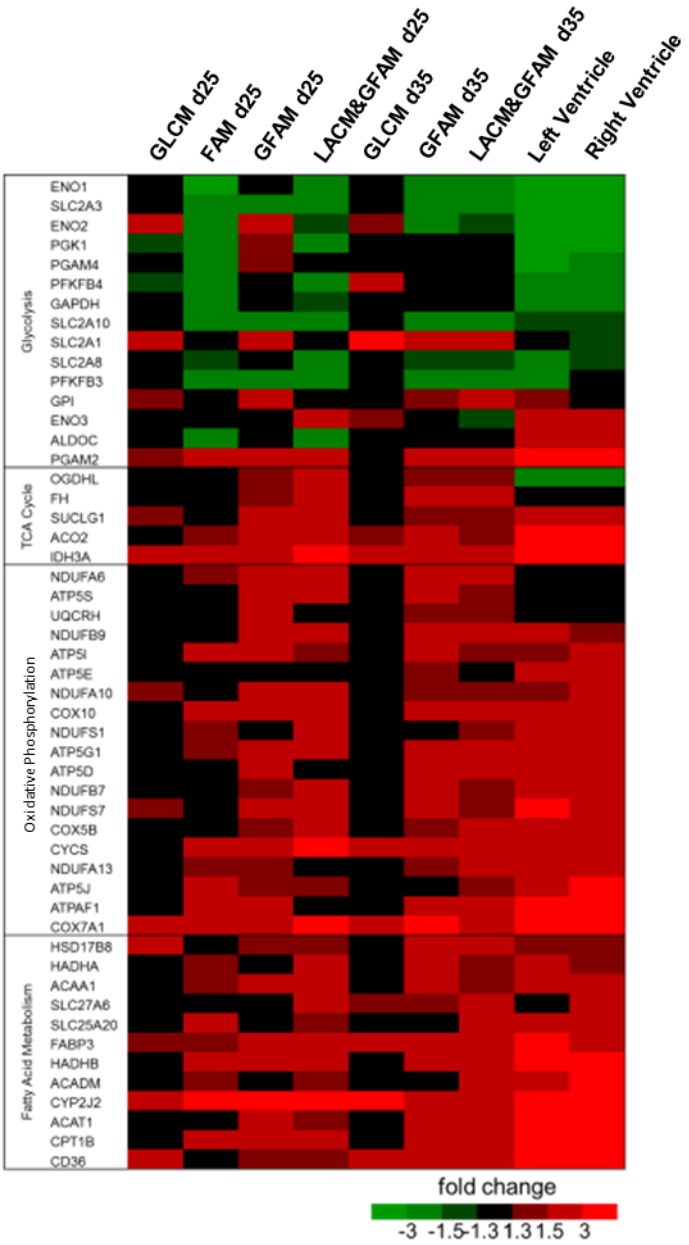

Figure S1 - Effect of culture media composition on metabolic gene expression. Heat map of differentially expressed genes associated with metabolic pathways. Heatmap shows averaged values from n=2. In all analyses, genes were considered enriched based on a fold difference in expression (FC) ≥1.3 when compared with d15. Green and red represent down- and up-regulation, respectively.